VOLUME 22, 1960/61, No. 7 pp. 217-244 Published 5th April 1961

Philips Technical Review

DEALING WITH TECHNICAL PROBLEMS
RELATING TO THE PRODUCTS, PROCESSES AND INVESTIGATIONS OF
THE PHILIPS INDUSTRIES

PROPERTIES AND APPLICATIONS OF INDIUM ANTIMONIDE

by R. E. J. KING*) and B. E. BARTLETT*).

546.682.'86

The increasing demand for photoconductive cells which extend their sensitivity range into the far infra-red, has led to the construction of two new photocells based on crystals of indium antimonide.

In this article the preparation of InSb crystals and the construction and performance of photocells based on InSb are described. Mention is also made of the use of InSb in Hall generators. These and other devices will be discussed in a forthcoming article in this journal.

In recent years a search has been made for semiconductors to supplement silicon and germanium for use in electronic applications. Since no other elements appear particularly useful, interest has been focussed on compounds. Most work has been done on compounds of elements from group III and V of the periodic table, such as GaAs, GaP, InSb, etc. Of these compounds, indium antimonide has been studied most intensively [1]), because its properties make it particularly suitable for a number of applications. In addition, the problems involved in the preparation of InSb are more tractable than those encountered with other, similar, compounds. Photocells, Hall generators and other devices based on InSb are already being manufactured by a number of factories, amongst others the Mullard division at Southampton.

Properties of InSb

Optical and electrical properties

In *Table I* is shown part of the periodic table of the elements. The elements within the columns of the table have roughly similar chemical properties because they have the same number of outer shell valency electrons.

The elements in column IVA, with the exception of lead, are found to be semiconductors and crystallise in the diamond configuration by forming four tetrahedral bonds. InSb forms the same type of structure utilising the three valence electrons of indium and the five of antimony to give the four bonds. Consequently the electrical and optical properties of the material are qualitatively similar to those of germanium and silicon. However, the magnitudes of the important parameters underlying the physical properties of the bulk material are different.

Table I. Groups IIIa, IVa and Va of the periodic table of elements.

IIIA	IVA	VA
B 5	C 6	N 7
Al 13	Si 14	P 15
Ga 31	Ge 32	As 33
In 49	Sn 50	Sb 51
Tl 81	Pb 82	Bi 83

4114

Two important quantities which affect the optical and electrical properties of the material are the *energy gap* and the *mobility of the charge carriers*. These will now be considered.

In solids there are *bands* of permissible energies for electrons in contrast to the discrete electron energy *levels* permissible in separate atoms. These bands

*) Mullard Radio Valve Co., Southampton Works.

1) A. N. Blum, N. P. Mokrovski and A. R. Regel, J. tech. Phys. (Moscow) **21**, 237, 1951; H. Welker, Z. Naturf. **7a**, 744, 1952 and **8a**, 248, 1953; R. Gremmelmaier and O. Madelung, Z. Naturf. **8a**, 333, 1953; H. Weiss, Z. Naturf. **8a**, 463, 1953.

are separated by forbidden ranges of energy. Now in a semiconductor the highest occupied energy band is exactly filled by the valence electrons available. Energy must be supplied — e.g. thermal, electrical or optical energy — to excite an electron from this band (the valence band) to the next (empty) band of higher electron energy (the conduction band). The energy separating these two bands is termed the "energy gap". (The greater this gap, the more the semiconductor approximates to an insulator.) Electrons with energies within a full band cannot carry any current but after such an excitation both the electron in the conduction band and the "hole" left in the valence band can conduct. When excitation can be achieved by optical energy, the material has the characteristics of a photoconductor.

In *Table II* the energy gaps of Ge, Si and InSb are compared. It is seen that the energy gap of the latter material is small, much smaller than that of Ge and Si. A consequence of this small energy gap is that radiation of quite long wavelengths is absorbed: the optical absorption edge of InSb is at 7.5 μ, as compared with 1.7 μ for Ge and 1.2 μ for Si.

Thus photoconductive cells covering the wavelength range from the visible to 7.5 μ can be made from InSb, utilising conduction changes due to carriers generated optically by excitation from the valence to the conduction band.

Table II. Some properties of germanium, silicon and indium antimonide.

	Ge	Si	InSb
Band gap (eV)	0.72	1.1	0.18
Intrinsic carrier concentration at 300 °K (cm^{-3})	2.5×10^{13}	6.8×10^{10}	2×10^{16}
Electron mobility at 300 °K (cm^2/Vs)	3600	1300	70 000
Hole mobility at 300 °K (cm^2/Vs)	1700	500	1000

The *mobility* of charge carriers is the average drift velocity acquired per unit applied electric field intensity in the direction of the field. This property is important for two reasons:

1) It is a parameter determining performance in both photocells and Hall-effect devices.

2) It is relevant to the investigation and control of the purity of material produced.

In a perfectly periodic crystal lattice at zero absolute temperature the mobility of charge carriers would be infinite. However, at higher temperatures, thermal vibrations of the crystal lattice reduce the mobility. In addition, the forces associated with impurities interfere with the motion of the carriers and this "scattering" can also be important in determining the mobility in the material. In order to ensure that the InSb produced meets the design desiderata for photocells and other devices, it is essential that the purity of crystals be investigated and controlled.

Two types of impurities are of particular importance, namely donors and acceptors, which give rise to electrons (N-type semiconductor) and holes (P-type), respectively. In the presence of both types of impurities simultaneously, compensation occurs and it is the difference between the concentrations of the two types which is operative in determining the carrier concentration. The determination of this difference in concentrations (or net concentration) is complicated by the presence of carriers due to purely thermal excitation across the energy gap (*intrinsic* carriers). The concentration of such intrinsic carriers in a pure InSb crystal at room temperature is about 2×10^{16} cm^{-3}, as compared with only 2.5×10^{13} cm^{-3} and 7×10^{10} cm^{-3} for germanium and silicon, respectively. Therefore, in order to determine impurity concentrations of this order or less, it is necessary to reduce the intrinsic concentration by cooling.

On the other hand, there is a certain (small) amount of activation energy required to excite an electron from the energy levels associated with the impurities which in fact is the very means of detecting the presence of the impurities. The temperature at which measurements are made must therefore be sufficiently high for the impurities to be all ionised, but sufficiently low for the intrinsic carrier concentration to be considerably less than the impurity concentration. In practice for InSb, at present levels of purity, 77 °K (boiling point of liquid nitrogen) is a suitable temperature.

To obtain the necessary information about the impurity concentrations and the mobilities, both the conductivity and the Hall effect are measured [2]).

The electrical conductivity σ for an N- or P-type semiconductor is given by

$$\left.\begin{aligned}\sigma &= ne\mu_n \\ \text{or}\quad \sigma &= pe\mu_p,\end{aligned}\right\} \quad \ldots\ldots\ldots \quad (1)$$

e being the electronic charge, n and p the respective concentrations of electrons and holes and μ_n and μ_p their respective mobilities.

To evaluate separately the carrier concentrations and mobilities, a Hall-effect measurement is made.

[2]) See, for example, C. Kittel, Solid-state physics, 2nd Edn. p. 296, Wiley, New York 1957.

The Hall effect may be illustrated with the aid of *fig. 1.*

If a current I is passed along a rectangular specimen and a magnetic field B is applied at right-angles

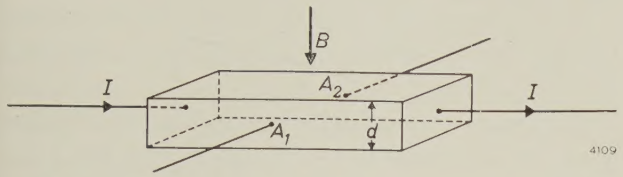

Fig. 1. The Hall effect. B is the induction of the applied magnetic field, I the current through the specimen of thickness d. A_1 and A_2 are the Hall-voltage contacts.

to the direction of current flow, then a potential difference is established in a direction perpendicular to both the field and the current directions. If contacts are made on the specimen at A_1 and A_2 this potential difference known as the Hall voltage, can be measured. The open-circuit Hall voltage V_{H_0} is given by the equation,

$$V_{H_0} = \frac{R_H I B}{d}, \quad \ldots\ldots \quad (2)$$

where d is the thickness of the specimen in the direction of the magnetic field. For a particular temperature R_H is a constant of the material and is known as the Hall coefficient. The above equation assumes that the ratio of length to breadth of the specimen is considerable greater than unity.

For an N- or P-type semiconductor, the Hall coefficient is:

$$\left.\begin{aligned} R_H &= -\frac{3\pi}{8}\,ne \\ \text{or} \qquad R_H &= +\frac{3\pi}{8}\,pe\,. \end{aligned}\right\} \quad \ldots\ldots \quad (3)$$

In *figs. 2* and *3* are shown the variation of the Hall coefficient and conductivity with temperature for two typical samples of InSb, the one being P-type and the other N-type, at low temperatures. Eq. (3) gives the electron or hole concentration, giving information on the difference between the concentrations of donors and acceptors. From the values of n and p and using eq. (1), the mobility of the carriers can be found.

In many cases, the mobility of the carriers may be wholly or almost wholly determined by their scattering by impurity atoms. Under these conditions the *total* impurity concentration may be determined by comparison with scattering theory [3]).

[3]) R. B. Dingle, Phil. Mag. **46**, 831, 1955.

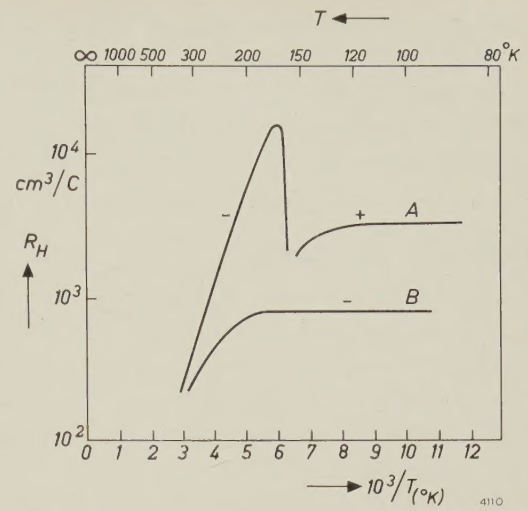

Fig. 2. Variation of Hall coefficient of (A) P-type and (B) N-type InSb with temperature. At temperatures below about 160 °K the Hall coefficient of sample (A) is positive. The high ratio of electron to hole mobility in indium antimonide causes the Hall coefficient to be negative at temperatures above 160 °K when it is a "mixed" conductor i.e. both electrons and holes are making a significant contribution to the conduction process. At higher temperatures both curves A and B approximate to the same straight line, which represents the intrinsic material.

From the Hall measurements, and using eq. (3), the *difference* in impurity concentrations is found. Hence the individual concentration of both acceptors and donors may be separately estimated.

From Table II it can be seen that the electron mobilities encountered in InSb are high compared with Ge and Si, being typically 70 000 cm²/Vs at room temperature. At 77 °K values as high as 650 000 cm²/Vs have been observed. The highest hole mobility observed at 77 °K is 10 000 cm²/Vs, and values deduced for room temperature may often reach 700-1000 cm²/Vs.

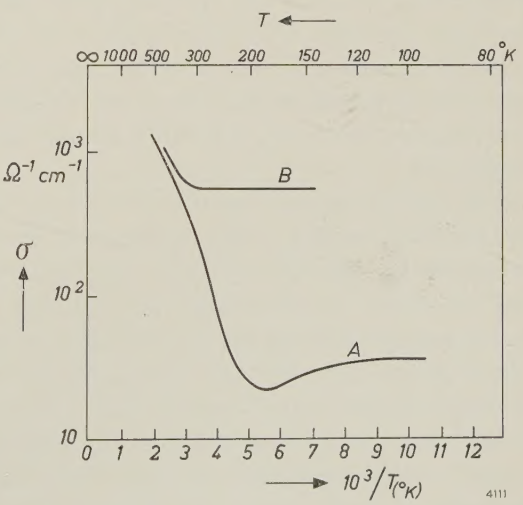

Fig. 3. Variation of conductivity of (A) P-type and (B) N-type InSb with temperature. For higher temperatures the material becomes intrinsic which is indicated by the fact (as in fig. 2) that curves A and B approximate to the same line.

A consequence of these high mobilities is that InSb displays large magnetoresistance effects [4]). A further consequence is that the power efficiency of Hall generators made from InSb is high compared with similar devices manufactured from Ge or Si.

Recombination and trapping

Non-equilibrium carrier concentrations in the bulk of semiconductor materials can be achieved by injection of carriers at contacts or by irradiation of the material with light of such a wavelength or wavelengths that valence electrons can be excited into the conduction band (leaving holes in the valence band) after acquiring energy from a photon-electron interaction. The first-mentioned process — injection at contacts — is made use of in diodes and transistors. The second process is made use of, as stated earlier, in photoconductors (photo-resistors).

After these processes the bulk of the material remains electrically neutral (no space charge is built up). When the process of injection or radiation is stopped, the concentrations return to equilibrium in a time which is in general long compared with the space-charge relaxation time when electrical forces accelerate the process of returning to equilibrium. The time for return to equilibrium is related to the *lifetime* of the charge carrier, i.e. the time that an electron remains in the conduction band, or a hole in the valence band, after excitation, and is, in general, determined by the probabilities of *recombination* and *trapping*. The first is the process of returning of an electron to the valence band by recombining with a hole. The second is the process of being "trapped" by a trapping centre and thus becoming immobile. As with transistors, the operation of photo-resistors depends on the existence of a *finite* lifetime of excess injected carriers in the material. The signal obtained from a photoconductive cell of given geometry is directly proportional to this lifetime.

In InSb, in contrast to Ge and Si, it is not at present possible to obtain non-equilibrium carrier concentrations in the bulk material, at room temperature or higher temperatures, by injection of carriers at contacts. To obtain injection it is necessary that a potential barrier is present at the contact to prevent the flow of one type of carrier into or out of the material. Consequently, it is not possible at present to make transistors or diodes from InSb for operation at room-temperature and above.

The room-temperature lifetime of excess carriers in InSb is *not* governed by traps and recombination centres, as in Ge or Si, and it is, at present, uncertain whether the recombining electron loses its energy in the form of radiation (radiative recombination) or by the Auger effect [5]) in which it loses its energy to another electron in the conduction band (see *fig. 4*). At 300 °K, typical lifetime values for InSb are about 5×10^{-8} sec.

At lower temperatures other mechanisms determine the recombination [6]). In particular, the presence of traps in the bulk or on the surface is important. These mechanisms can be studied by measurements of the photoconductive and photomagneto-electric type.

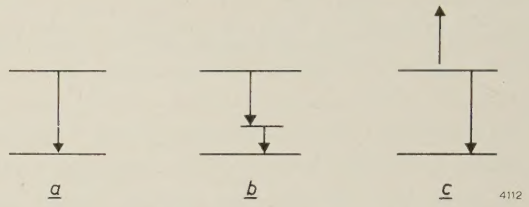

Fig. 4. Recombination processes.
a) Radiative recombination. An electron in the conduction band recombines directly with a hole in the valence band, accompanied by the emission of a photon.
b) Recombination via a trap. An electron is "trapped" in an energy level in the forbidden zone, and after some time recombines again with a hole in the valence band.
c) Auger effect. An electron in the conduction band falls back to the valence band and the energy which comes free is transferred to another conduction electron, lifting the latter to a higher energy level in the conduction band.

Preparation of InSb

As InSb is a compound, its preparation differs somewhat from the preparation of the elemental semiconductors. It has the advantage that the two constituent elements may be purified before the compound is prepared and impurities difficult to remove from the compound may be removed from the elements themselves, but there is the possibility that non-stoichiometry (excess of one of the elements in the compound) will occur. In fact, there is no evidence for the solubility of significant amounts of either excess In or excess Sb in solid InSb, although it is not certain whether this is still true for very low concentrations of the order of 10^{14} cm^{-3}.

For the efficient production of reproducible devices from InSb, there are three requirements to be met in the material production process. These are: 1) high degrees of purity, 2) single crystals and 3) uniformity of material over useful working volumes.

[4]) H. P. R. Frederikse and W. R. Hosler, Phys. Rev. **108**, 1136, 1957.

[5]) A. R. Beattie and P. T. Landsberg, Proc. Roy. Soc. **A 249**, 16, 1959.

[6]) D. W. Goodwin, Report of the meeting on semiconductors, Physical Society and British Thomson-Houston Ltd. (Rugby, April 1956), p. 137.

The fulfilment of the first of these requirements ensures that the high mobilities realisable in InSb can be utilised in devices such as the Hall generator. Also doping the material to levels set by design considerations for photocells can be readily accomplished if pure starting material is employed.

Single crystals are necessary if thin foils or filaments are to be prepared by anodic etching (polycrystalline material is preferentially etched at grain boundaries) and uniformity is essential for the attainment of uniform photoconductive response along a filament of InSb.

To meet the above-mentioned requirements, the preparation of InSb, as with Ge and Si, is carried out in two stages: the production of high purity polycrystalline ingots and the growth of uniform single crystals from this material. For the purification, use is made of the principle of zone refining developed by Pfann [7]). In this process a molten zone is repeatedly passed in the same direction along a bar of the material to be purified. Impurities tend to be either more soluble in the solid than in the melt or vice versa and are swept to the one or the other end of the bar. The property of differing solubility in the solid and melt can be put on a quantitative basis by defining the distribution coefficient for a given impurity:

$$k_0 = \frac{\text{concentration of impurity in the solid}}{\text{concentration of impurity in the melt}}$$

for thermodynamic equilibrium conditions between the solid and melt at the molten zone. If k_0 is less than 1, impurities concentrate in the molten zone and are swept to the end of the bar which freezes last, while if k_0 is greater than 1 they tend to remain in the solid and the molten zone contains less impurities than the starting material. In this case, the end which freezes last contains the purest material. Zone refining is impossible if k_0 is unity.

Polycrystalline ingot preparation

The starting materials for the preparation are commercial high purity indium and antimony, each containing about one part per million of impurities. Experiment has shown that, for the production of indium antimonide of the highest purity, the commercially pure *antimony* must be purified further by zone refining in a hydrogen atmosphere before the compound is prepared. During this zone refining, impurities (probably S or Se) which are not readily zoned out of InSb, are removed.

As regards the *indium*, zinc and cadmium are present in the commercially pure metal and must be removed as they are acceptors in InSb [8]). Both have k_0's so near to 1 in InSb that zone refining is inefficient, but fortunatly they both have sufficiently high vapour pressures to allow them to be removed by evaporation. Most of the zinc and cadmium is removed by baking the indium under vacuum at 800 °C in the crucible in which the compound is prepared. The chemically equivalent quantity of antimony, correct to about 1%, is then added. The crucible is sealed off under vacuum and the contents fused together at 750 °C for some hours. After freezing, the compound is further purified by giving the ingot thirty zone passes through an eddy-current heater. During this process, not only are a large number of impurities concentrated at the two ends of the bar but also Zn and Cd are condensed on the upper part of the crucible which remains relatively cool.

Hall measurements show that 65% of the ingot has a difference of donor and acceptor impurity concentrations approximately equal to 10^{14} cm^{-3}. The remaining impurity has not been identified. Harman [9]) has suggested that it is tellurium originating in the indium but this has not been confirmed.

Preparation of single crystals

Single crystals are pulled by the Czochralski method [10]), in which a rotating seed crystal is slowly withdrawn from a melt of the material. A typical crystal puller is shown in *fig. 5*. Crystals are grown under vacuum at a rate of 2.5 cm/hour and a rotation rate of 120 rpm. It has been observed that donor concentrations are markedly lower under vacuum than when pulling in a gaseous ambient. During pulling there is a relatively large loss of antimony (about 0.1%), but the solubility of indium in indium antimonide is evidently sufficiently low that the stoichiometry of the crystal is not appreciably affected. Undoped crystals, which are *N*-type, due to residual impurities, have an electron concentration of approximately 10^{14} cm^{-3} and can have mobilities up to 650 000 cm^2/Vs at 77 °K as mentioned earlier.

Germanium is an acceptor in InSb and is used for doping in preference to Zn and Cd, which are volatile in vacuum. It has a k_0 of 0.02, giving an acceptor concentration varying by a factor of 2 during the pulling of the first 50% of the melt.

[7]) W. G. Pfann, J. Metals **4**, 347, 1952. See also J. Goorissen, Philips tech. Rev. **21**, 185, 1959/60 (No. 7).

[8]) J. B. Mullin, J. Electronics and Control **4**, 358, 1958.

[9]) T. C. Harman, J. Electrochem. Soc. **103**, 128, 1956.

[10]) J. Czochralski, Z. phys. Chem. **92**, 219, 1917. See also B. Okkerse, Philips tech. Rev. **21**, 340, 1959/60 (No. 11).

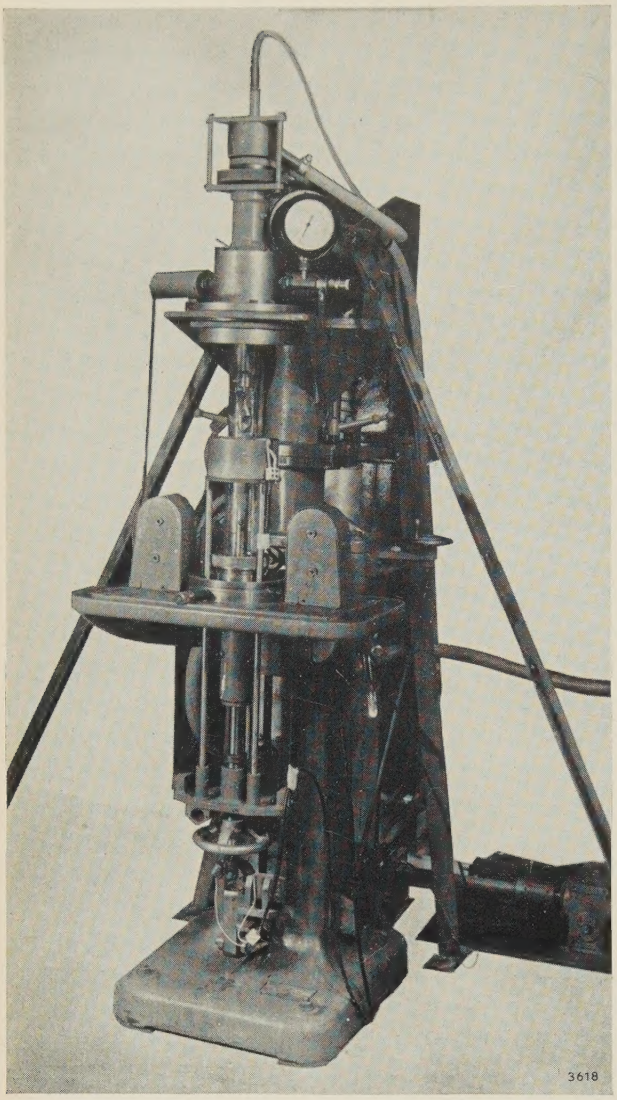

Fig. 5. Crystal puller used for production of single crystal InSb. The crucible is heated by radiation from a resistance coil not in contact with the crucible.

At doping levels greater than 10^{15} cm^{-3} the resistivity across crystal slices is uniform to within about 25% on crystals pulled on the (111) plane, i.e. when a (111) face of the crystal is in contact with the melt. At lower doping levels, larger variations are observed, although sufficient uniformity can be maintained to produce material with a *P*-type resistivity at 77 °K of 10 Ωcm (i.e. hole concentration of 10^{14} cm^{-3}). More uniform crystals are, however, easily produced by pulling on the (211) plane, when resistivities up to 100 Ωcm with 10% variation across slices can be obtained. Hulme and Mullin [11]) have shown that the variation in resistivity in crystals pulled on the (111) plane is caused by the k_0 of the residual *N*-type impurity varying across the (curved) growing interface due to the presence of (111) facets. If the crystal is pulled on the (211) plane, (111) facets and consequent changes in resistivity do not occur.

Fig. 6 shows a single crystal of InSb grown on a (211) plane.

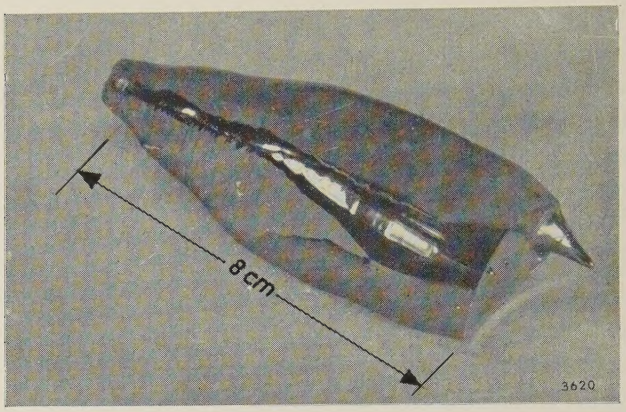

Fig. 6. Single crystal of InSb grown on the (211) plane. It can be seen that the cross-section is not circular. This is due to the different growth velocities in the different crystallographic directions.

Applications of InSb

Photoconductive cells; general

As mentioned above, the small energy gap of InSb makes it particularly suitable for use in infra-red detectors. Photocells using InSb have been made utilising photoconduction, the photomagnetoelectric effect or the photovoltaic effect. The photoconductive cell is the simplest of these.

Two photoconductive cells will be discussed. The first of these, the ORP 10, is a detector which is operated at or near room temperature. This cell can be used to detect infrared radiation up to a wavelength of 7.5 μ. This extends the sensitivity range of the existing set of infrared detectors, the lead sulphide (PbS), lead selenide (PbSe) and lead telluride (PbTe) cells with their respective limits of 3.5 μ, 5 μ and 6 μ.

The second InSb cell, the ORP 13, is designed for operation at liquid-nitrogen temperature. This is a much more sensitive cell but it has a reduced spectral sensitivity, operating to 5.5 μ, which is comparable with the PbTe photocell.

The InSb cells have shorter time constants than those made from other materials. Thus they are particularly suited for applications where a fast response is required, e.g. military infra-red systems or fast automatic recording instruments.

Photoconductive detectors are usually operated by passing direct current through the sensitive filament or layer. The change in current resulting

[11]) K. F. Hulme and J. B. Mullin, Phil. Mag. **4**, 1286, 1959.

from the increase in conductance during illumination is then amplified and measured. In order to facilitate amplification, the incident radiation is usually chopped at a suitable frequency, often near 1 kc/s.

When the performances of detectors at a given wavelength and in a particular system are compared, there are two cell characteristics which are important. These determine the overall signal-to-noise ratio of the two cases, (*a*) system noise large compared with cell noise, and (*b*) system noise small compared with cell noise.

For case (*a*) the performance is determined by the *responsivity*, defined as the detector output voltage per unit incident signal power.

In case (*b*) the *noise equivalent power* (N.E.P.) is important. This is sometimes termed minimum detectable energy. The N.E.P. is the incident radiation power for which the signal equals the cell noise. The N.E.P. is referred to a particular bandwidth, usually 1 c/s.

The ORP 10 detector

This infra-red photocell is illustrated in *fig. 7*. It consists of a 10 μ thick strip of InSb attached to a copper mount drilled to facilitate mounting on a heat sink. The sensitive area is a rectangle 6 mm × 0.5 mm. The dark resistance of the cell is 100 Ω, which is suitable for use with transistor amplifiers.

If, at room temperature, I photons per unit area per second are incident on a filament of InSb of width b and resistance R, the steady electric field in the filament being E, then the open-circuit signal voltage V_s is given by

$$V_s \propto I\, e\, (\mu_n + \mu_p)\, \tau E R b\,, \quad \ldots \quad (4)$$

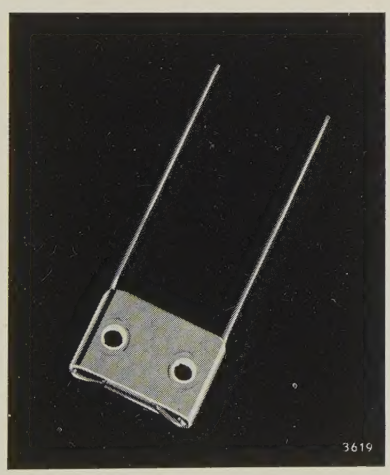

Fig. 7. The Mullard photoconductive cell ORP 10. The InSb element is visible on the edge of the drilled copper block. The leads to the InSb run though the copper block which thus serves as a heat sink during the soldering of connections.

where τ is the lifetime of the charge carriers. If the lifetime in the material was independent of the carrier concentration the signal could be increased by increasing the resistivity, e.g. by doping the material with acceptors. However, it has been found that there is a decrease in lifetime which tends to offset any increase in resistance obtained by doping.

Doping with acceptors increases the resistivity, which is given by the equation $\varrho = (ne\mu_n + pe\mu_p)^{-1}$ when both electrons and holes participate in the conduction process. Other conditions which hold are $np = n_i^2$ and $p - n = n_A$, where n_i is the intrinsic carrier concentration and n_A the acceptor concentration. With the aid of these relationships it can be shown that ϱ_{max} occurs when

$$n_A = n_i \left(\frac{\mu_n - \mu_p}{\sqrt{\mu_n \mu_p}} \right)$$

and *not* for $n_A = 0$, i.e. intrinsic material.

The noise is found to be always less than twice the Johnson noise whose voltage is denoted V_n. Now

$$V_s / V_n \propto \frac{(\mu_n + \mu_p)\, \tau}{\sqrt{\sigma}} \quad \ldots \quad (5)$$

for a given power dissipation in the filament. This quantity decreases with increased doping: intrinsic or near intrinsic material is therefore used for the cell.

In *Table III*, the characteristics of this cell are compared with those of other photoconductive cells.

The ORP 10 detector possesses the following special features:

1) Rapid measurements can be made of radiations with wavelengths up to 7.5 μ. In this wavelength range the cell therefore supplants thermal bolometer detectors, which are rather slow.

2) The cell is particularly suitable for *spectrometer* applications. The form of the InSb element — a narrow strip — and its mounting permit an array to be used and simultaneous observation of several bands seems feasible. Observations for extended periods of time may be made without complicated cooling arrangements. The wide wavelength range, which includes the main atmospheric absorption bands, permits the study of fundamental absorption bands of many chemical groups without the use of thermal bolometer detectors. The latter are not conveniently incorporated into automatic equipment.

3) The cell is sensitive to the thermal radiation from bodies at relatively low temperatures, e.g. the radiation from 1 cm² of a black body at 40 °C can be easily measured at a range of 40 cm.

Table III. Comparison between some photoconductive cells.

Cell category	Type No.	Effective sensitive area (mm^2)	Spectral range (μ)	Peak response (μ)	Time constant (μsec)	Dark resistance (kΩ)	Sensitivity, noise and figure of merit			
							Radiation	Sensitivity	Noise equivalent power per unit bandwidth (10^{-9} W)	Figure of merit D^* (cm/μW)
PbS	61 SV	36	0.3 - 3.5	1.8 - 2.8	75	1000-4000	Tungsten lamp at 2700 °K	3mA/lumen	0.055	11000
							Black body radiation at 200 °C	180 μV/μW	5	120
PbSe	61 RV	6	1.0 - 5.0	2.0 - 4.3	<1.0	15 - 100	Monochromatic at 4 μ	15 μV/μW	<8.5	>29
InSb	ORP 10	3	0.6 - 7.5	5.0 - 7.2	<1.0	0.1	Monochromatic at 6 μ	0.3 μV/μW	<4	>43
							Black body radiation at 200 °C	0.36 μV/μW	<10	>17
InSb liquid-nitrogen cooled	ORP 13	3.5	0.6 - 5.5	4.5 - 5.0	<10	20 - 40	Monochromatic at 4 μ	14 mV/μW	<0.02	>9000
							Black body radiation at 200 °C	2.4 mV/μW	<0.12	>1500

$D^* = (\text{NEP})^{-1} \times (\text{area})^{\frac{1}{2}}$ and is a figure of merit for photocells when used for detecting low-level radiation [12]). D^*, unlike NEP, is independent of photocell sensitive area and represents a sound basis for comparison of photocells of different area.

The ORP 13 cooled photoconducting cell

Detectors with the same light-sensitive area as the ORP10 have been developed for operation at liquid nitrogen temperature, see *figs. 8* and *9*.

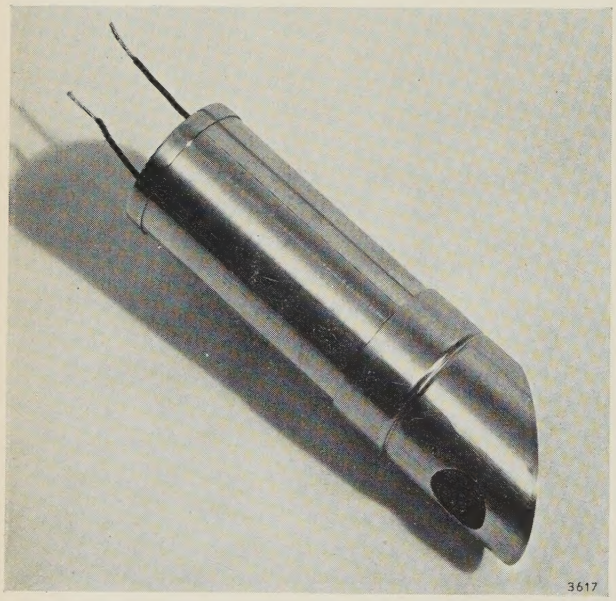

Fig. 8. The Mullard cooled InSb cell ORP 13, in its metal housing.

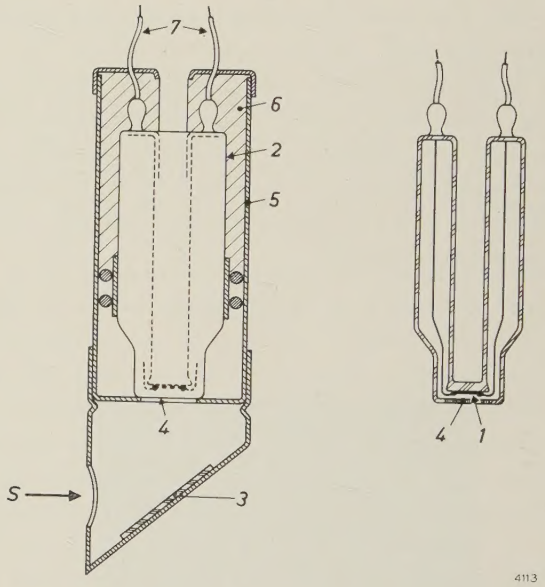

Fig. 9. Construction of the cooled InSb cell. The InSb element *1* is cooled by filling the Dewar flask *2* with liquid nitrogen. A demountable mirror *3* facilitates the measurement of horizontally incident radiation. A sapphire window *4* is sealed to the Dewar flask just in front of the InSb strip. The Dewar is housed in a metal tube *5* containing a resilient filling *6*. The leads *7* of the cell pass through glass-metal seals in the Dewar flask.

The values of the parameters in equation (4) are modified at this temperature. *P*-type material is used because the hole mobility is much less than the electron mobility — this gives high resistivity,

[12]) R. C. Jones, Proc. Inst. Radio Engrs. **47**, 1495, 1959.

about 30 times the room temperature value, and therefore high cell resistance and large signals. The process determining the lifetime of excess holes and electrons is *electron* trapping. The signal voltage V_s is given by

$$V_s \propto I e \mu_p \tau_p R E b, \quad \ldots \quad (6)$$

where τ_p is the hole lifetime.

At this temperature the resistivity would be *decreased* by doping because there are a negligible number of intrinsic carriers present. The product $\mu_p \tau_p$ would also be decreased by doping. The purest possible *P*-type material is therefore used.

In this cell the noise appears to be semiconductor "fluctuation noise" (fluctuations in the recombination process). Using *P*-type material of resistivity at 77 °K of up to 10 Ωcm the characteristics given in Table III are obtained.

After the cell has been exposed to visible radiation while cooled, a quasi-permanent change in the dark resistance takes place. The original resistance value may be re-attained by allowing the cell to warm to room temperature and then cooling it once more.

Owing to its great sensitivity this cooled detector is a useful addition to the present range of photoconductive cells.

Hall generators

Indium antimonide has been quite widely used as the basis of Hall generators. These are devices in which the output signal is proportional to the product of two currents, either of which may be steady or variable. One of the currents is passed through a plate of the material (as in the measurement of the Hall effect, see page 219) and the other is fed into the winding of an electromagnet producing the magnetic field on the plate. The output voltage from the Hall probes is then proportional to the product of the two currents. A load may be inserted between the Hall probes and power drawn in the output circuit.

Many applications and refinements of these devices have been described in the literature. Considerations concerning this type of device will form the subject of a forthcoming article in this journal.

The large magnetoresistance effect in InSb has likewise led to a number of applications, including displacement gauges and tiny measuring probes for high intensity magnetic fields. In these devices a disc geometry is often used for the InSb element; this arrangement gives a large change in resistance when a magnetic field is applied. The magnetoresistance effect is proportional to the square of the carrier mobility, thus InSb is particularly suitable for such applications.

Summary. Indium antimonide is a compound with semiconducting properties. The small energy gap makes it a good photoconductor. This has led to the construction of photoconductive cells with either long-wavelength response (the Mullard ORP 10 to 7.5 μ) or high sensitivity (the Mullard ORP 13, cooled with liquid nitrogen, with a sensitivity of 14 mV/μW at 4 μ). Moreover the lifetime of the free charge carriers is very short, so that InSb cells are very fast: the time constant of the ORP 10 is <1 μsec, that of the ORP 13 is <10 μsec.

The electron mobility is observed to be very high (650 000 cm²/Vs at 77 °K), making InSb also particularly suited for use in Hall generators. The large magnetoresistance effect in InSb has likewise led to a number of applications, including displacement gauges and tiny measuring probes for high intensity magnetic fields.

Very pure single crystals of InSb are prepared from previously purified indium and antimony. The compound is further purified by zone melting, after which single crystals are formed by pulling from the melt on the (211) plane. Doping with Ge (for example) gives *P*-type material, while without doping it is *N*-type because of residual impurities.

SOLID-STATE RESEARCH AT LOW TEMPERATURES

II. ELECTRON CONDUCTION IN METALS AND SEMICONDUCTORS [1])

by J. VOLGER.

536.48

Following the previous article in this series, which was mainly introductory, the article below deals with various recent investigations on solids at low temperatures. Except for the first one, all these investigations were carried out at Philips Research Laboratories in Eindhoven.

Electrical conduction in metals at low temperature

When a metal is cooled from room temperature, its resistance at first decreases more or less linearly with temperature. However, upon reaching the temperature region below about 50 °K — the actual temperature differs from one metal to another — the resistance curve bends over and, at very low temperatures, becomes virtually horizontal (*fig. 1*). Near absolute zero the value of the resistance is not zero, but has a finite value known as the residual resistance. The magnitude of this residual resistance depends on the concentration of the impurities in the metal — the purer the metal, the lower the residual resistance — and also on the physical lattice imperfections. Theoretically, the resistivity of a metal is regarded as the sum of a component ϱ', caused by thermal vibrations of the crystal lattice, and a component ϱ'', due to scattering of the electrons (regarded as wave packets) by the foreign atoms. The magnitude of ϱ' obviously depends on the temperature, and becomes zero when T approaches the absolute zero point of temperature. The residual resistance is thus entirely determined by ϱ''. Provided the impurity concentration is not unduly large, ϱ'' is independent of temperature (Matthiessen's rule). The value of ϱ', apart from being temperature-dependent, is almost entirely governed by the nature of the metal and is not significantly affected by the impurity concentration.

We shall now discuss some examples of investigations concerning the contributions made to the resistivity by physical lattice imperfections (in aluminium and in copper) and by impurities (carbon in iron). To yield results, these investigations had to be carried out at such a low temperature that the value of the resistivity was primarily determined by ϱ'' (viz. at 20.4 °K, the boiling point of hydrogen at 1 atm).

[1]) Sequel to the article: J. Volger, Solid-state research at low temperatures, I. Introduction, Philips tech. Rev. **22**, 190-195, 1960/61 (No. 6). This article is further referred to as I.

The influence of physical lattice imperfections on the electrical resistivity of highly purified aluminium

As our first example we shall briefly describe an investigation concerning aluminium [2]). The results obtained give a clear picture of the separate influences of the point defects (vacancies, interstitial atoms) and linear lattice defects (dislocations).

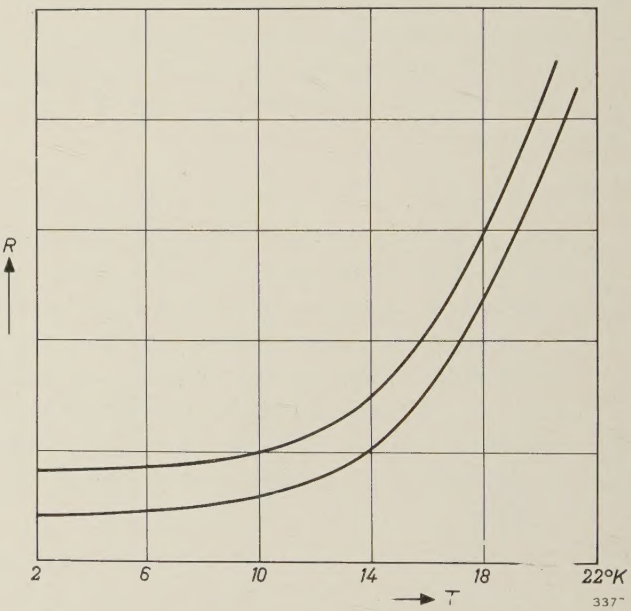

Fig. 1. The variation of the electrical resistance R with temperature of two sodium samples of differing purity. Below the relatively low temperature of 10 °K, there is hardly any further decrease in R. The purer sample has the lower residual resistance (after D.K.C. MacDonald and K. Mendelssohn, Proc. Roy. Soc. **A 202**, 103, 1950).

Three experiments were done. The first consisted of plastically stretching by 10% an annealed aluminium wire. (Annealing removes a considerable proportion of the lattice imperfections produced during the drawing process or during a previous elongation [3]).)

[2]) M. Wintenberger, C. R. Acad. Sci. Paris **242**, 128, 1956 and **244**, 2800, 1957.

[3]) For further particulars of this subject, see H. G. van Bueren, Lattice imperfections and plastic deformation in metals, Philips tech. Rev. **15**, 246-257 and 286-295, 1953/54.

The resistivity, measured at 20 °K, was found to have increased. After about two hours, part of the excess resistivity had disappeared, the other part proved to be permanent. From the two other experiments it was concluded that the temporary part of the excess resistivity was due to the point defects caused by stretching, which gradually disappear, and that the remaining part must be attributed to an increase in the number of dislocations. When the number of point defects (vacancies) was raised, *without* appreciably increasing the dislocation density — this can be done by heating the metal almost to the melting point and then quenching it rapidly in air — the excess was found after some time to have almost completely disappeared, even though it was originally roughly five times greater than in the first experiment. The fact that the *rate* at which the excess resistivity disappeared was much less here than in the first experiment is also in agreement with the explanation given above, since the "sinks" into which the point defects can vanish are, of course, the dislocations [4]), and the rate at which they vanish is clearly less for a smaller dislocation density. Confirmation of all this was obtained from a third kind of experiment, in which the wire was again first heated and quenched but afterwards stretched. The excess now proved to be somewhat greater than in the previous experiment — additional vacancies had now been created in *two* ways — but it decreased at the same rate as in the first experiment. Here again part of the excess was permanent, and it was roughly of the same magnitude as in the first case. Both the rate of decrease of the temporary part and the magnitude of the permanent part can be related to the dislocation density.

Magnetoresistance of copper

It has been known for some time that the electrical resistance of a metal undergoes a slight change when the metal is subjected to a magnetic field (magnetoresistance). In the case of well-annealed samples of the same metal the fractional change in resistance $\Delta\varrho/\varrho_0$ plotted against H/ϱ_0 always yields the same curve, irrespective of the temperature and of the value of the residual resistance ($\Delta\varrho$ is the change in the resistivity, ϱ_0 is the resistivity in the absence of a magnetic field, and H the magnetic field-strength). It has been found that, although this rule (Kohler's rule) is valid for the residual resistance due to impurities and other point defects, it does not hold for the contribution from the dislocations [5]). The results obtained from measurements of this effect are collected in *fig. 2*. The curves show the relation between the above-mentioned ratios as found for copper wire. It can be seen that the

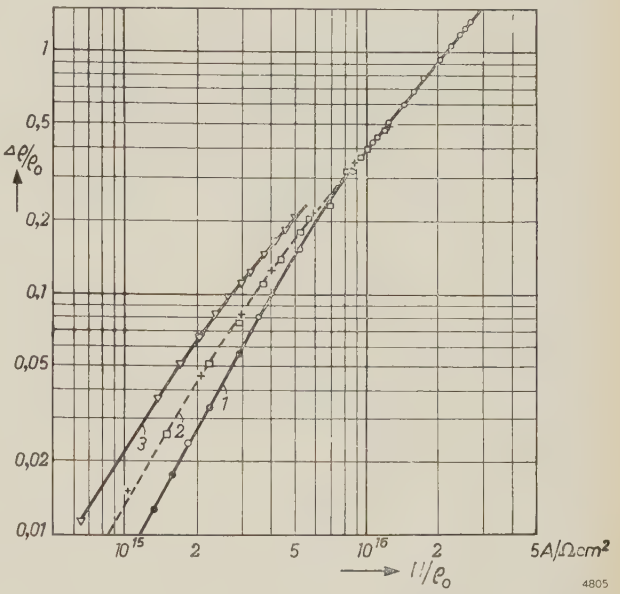

Fig. 2. The way in which the magnetoresistance $\Delta\varrho/\varrho_0$ of a metal depends on H/ϱ_0 (H being the magnetic field) is not affected by point defects in the lattice, but it *is* affected by dislocations. This is illustrated here for copper. Curve *1* relates to annealed copper wire. The points for pure (●) and impure (○) material are seen to lie on the same curve. Curve *2* relates to pure copper wire which was plastically stretched 9.6% at 20 °K (points □) and also after subsequent heating at 220 °C (points +). It can be seen that curve *2* differs appreciably from curve *1*, particularly at low values of H/ϱ_0, and that this deviation is not eliminated by heating at 220 °C; to bring the wire back to resistance of curve *1* it has to be reannealed. Curve *3* relates to a wire of 0.5 mm diameter which, after annealing, was stretched to a diameter of 0.2 mm.

points for pure and impure copper indeed lie on the same curve, provided the wires have been annealed beforehand and then slowly cooled. After stretching (at 20 °K), however, the curve is seen to have shifted. On heating the wire to 220 °C — at which temperature the (physical) point defects are removed — no reduction in this effect is found. The effect can only be eliminated by *annealing*, that is to say by again reducing the dislocation density to the original value. This result, combined with that found from measurements of the recovery of the electrical resistance after stretching (in the absence of a magnetic field) led to the conclusion that Kohler's rule is valid only for the point-defect contribution to the resistance. The cause of this anomalous behaviour is thought to be the anisotropy of the scattering

[4]) See e.g. B. Okkerse, A method of growing dislocation-free germanium crystals, Philips tech. Rev. **21**, 340-345, 1959/60 (No. 11).

[5]) P. Jongenburger, Ned. Tijdschr. Natuurk. **22**, 297, 1956 (in Dutch).

power of dislocations. A theory based on this supposition [6]) has in fact yielded an effect of the right order of magnitude.

Finally, a remark on the fact that, where the plastic deformations are not excessive, the anomalous effect disappears when H is stronger than roughly 10^6 A/m. The radius of curvature of the orbits described by the electrons then decreases to about 10^{-3} cm, which is smaller than their mean free path. In a strong magnetic field, then, an electron may thus make one or more complete revolutions between two collisions, and it is conceivable that this will attenuate or completely eliminate the anisotropic effect of the dislocations [7]).

Electrical resistivity of iron contaminated with carbon

The way in which the residual resistance is affected by the impurity concentration is elegantly illustrated by the results of an investigation made on iron [8]). All resistivity measurements were done at 20 °K and at 20 °C (293 °K). First of all the ratio $\varrho_{293}/\varrho_{20}$ was determined for very pure iron [9]); the value found was 147 $\pm$ 2. If we compare this with the value 187 $\pm$ 5, found on a similar iron wire which was subsequently further purified by zone melting (11 $\times$), we get some idea of the considerable effect which the impurities have on the value of ϱ at low temperature. It is to be hoped that means will be found of using this effect conversely for the quantitative chemical analysis of traces of impurities at concentrations which cannot be detected, or only with great difficulty, by other methods.

The way in which ϱ'' depends on the carbon concentration C was found by measuring the resistivity of wires of different concentrations at the temperatures mentioned. Denoting the ratio of these resistivities, $(\varrho'_{20} + \varrho'')/(\varrho'_{293} + \varrho'')$, by p_c, and the ratio $\varrho'_{20}/\varrho'_{293}$ by p_z, we have that ϱ''/ϱ'_{293} is equal to $(p_c - p_z)/(1 - p_c)$. *Fig. 3* shows the results of the measurements. It is seen that the relation between ϱ'' and the concentration C can be represented by a straight line passing through the origin. This leads to the conclusion that the contributions of the carbon atoms to the scattering of the conduction electrons are additive; there is apparently no mutual interaction between the neighbouring carbon atoms. In view of the small carbon concentration and the correspondingly large average distance between the carbon atoms, this result is not surprising.

It may further be deduced from fig. 3 that the proportionality factor between ϱ''/ϱ_{293} and the carbon concentration (expressed in percentage by weight) is approximately 2.1 to 2.2. Measurements at a higher temperature, done by other workers [10]), yielded higher values. Matthiessen's rule, according to which ϱ'' is not dependent on temperature, is apparently valid only in a restricted temperature range. This was confirmed by measurements at 77 °K on the same iron wires used in the above investigation. These measurements resulted in a value of 2.55.

Superconductivity

Certain metals and alloys, and also certain metallic nitrides and carbides, exhibit the effect of superconductivity when their temperature is reduced to an extremely low value. Although this was discovered half a century ago (by Holst and Kamerlingh Onnes in 1911), progress towards a complete fundamental theory of the phenomenon has only been made in recent years [11]).

A superconductive material shows two characteristic properties: 1) the electrical resistance is

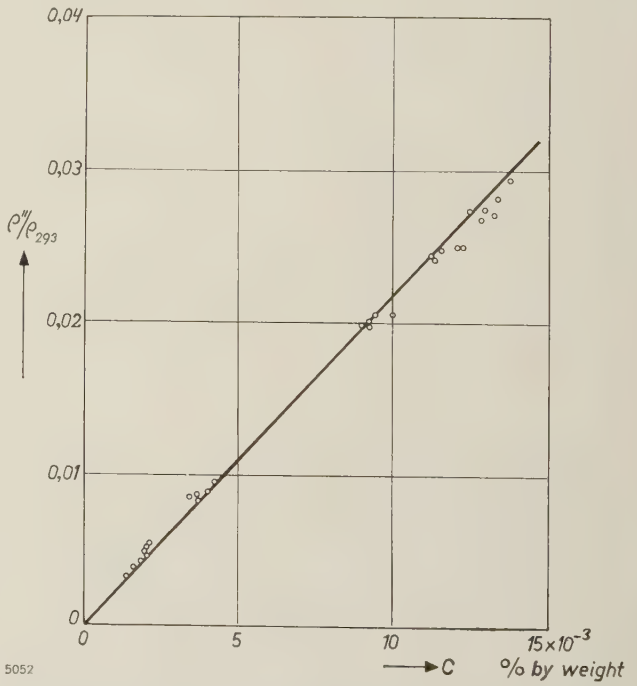

Fig. 3. The variation of the residual resistivity ϱ'' (expressed as a fraction of ϱ_{293}) with the concentration C of carbon dissolved in iron. The relation between ϱ'' and C is seen to be given by a straight line passing through the origin.

[6]) H. G. van Bueren, Philips Res. Repts. **12**, 1 and 190, 1957. See also reference [5]).

[7]) More recent measurements by Prof. Jongenburger will be published shortly in Acta Metallurgica.

[8]) Carried out by G. Baas of this laboratory.

[9]) For the method of preparation see J. D. Fast, A. I. Luteijn and E. Overbosch, Philips tech. Rev. **15**, 114, 1953/54.

[10]) W. Köster, in Arch. Eisenhüttenw. **2**, 503, 1928/29, and L. J. Dijkstra, in Philips Res. Repts. **2**, 357, 1947, found a value of 2.5 at 25 °C, W. Pitsch and K. Lücke, in Arch. Eisenhüttenw. **27**, 45, 1956, found a value of 2.75 at 22 °C.

[11]) See e.g. C. G. Kuper, Adv. Phys. **8**, 1, 1959 (No. 29) and I. M. Khalatnikov and A. A. Abrikosov, ibid. page 45.

zero (except in the case of alternating currents whose frequency exceeds a certain value), and 2) an external magnetic field penetrates only a very thin surface layer and is excluded from the bulk (the Meissner effect). The temperature below which a substance becomes a superconductor, the *transition temperature*, is changed by the application of an external magnetic field. The curve showing the relation between the transition temperature and the external field is shown in *fig. 4*.

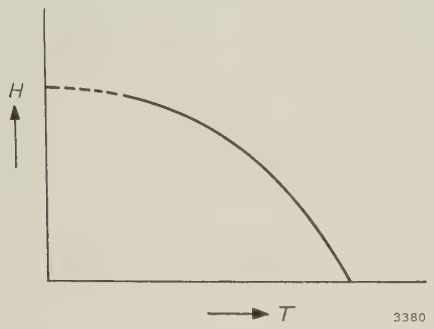

Fig. 4. Curve showing the transition point of a superconductor At a certain temperature T the material is superconductive only if the strength of the external magnetic field H is lower than the corresponding ordinate value of the curve.

Because of the complete absence of electrical resistance, there can be no electrical field inside a superconductor, for such a field would evidently give rise to an infinitely strong current. If a ring of superconducting material, placed in a magnetic field, is cooled to below the transition temperature corresponding to that field, and if the magnetic field is then switched off, a current is induced in the ring of such magnitude that the magnetic flux enclosed by the ring remains as it was. If the temperature is maintained below the transition point, this current persists for an unlimited time without becoming noticeably weaker. This persistent-current phenomenon has attracted attention in recent years, since it can be turned to use for storage elements in electronic computers.

The fact that the superconductivity can be removed and restored again by means of an external magnetic field is important in the design of storage elements, in connection with the write-in and read-out processes. But the phenomenon is of technical interest in itself, in that it can be used to make an electrical switching device which functions very roughly in much the same way as a triode [12]). The principle is illustrated in *fig. 5*. The "resistance" *a*, which is connected to the terminals *2* via the conductors *b*, is surrounded by a solenoid *c*. The temperature of *a* is kept just below the transition point, so that superconductivity occurs and the resistance between the terminals *2* is entirely determined by that of the leads *b*. If a current source is now connected to the terminals *1* which causes a current flow in *c* such that the resultant magnetic field removes the superconductivity of *a*, there will be an increase in the resistance between the terminals *2*. If the resistance of *a* is high in relation to that of *b*, the arrangement may be regarded as a switch.

The most suitable form of *a* is that of a straight strip of very small thickness. Its resistance R must obviously be high, but at the same time its inductance L as low as possible, since the speed with which the superconductivity state changes to the normal state, and vice versa, is greater the larger is the value of R/L. A long thin wire, which might be coiled to save space, is therefore out of the question.

In view of the extremely restricted choice of basic materials — there are not many superconductive materials, and boiling helium is the only suitable cooling bath — it was a long time before a strip could be made that adequately fulfilled the requirements. A particularly suitable material from the electrical viewpoint is tantalum. The transition point of bulk tantalum lies at 4.4 °K, which is only 0.2 °K above the boiling point of helium; this means that its superconductivity can be removed with a relatively weak magnetic field. If one tries, however, to make a thin strip of this material by vapour-deposition in vacuum, the strip usually acquires electrical properties so different from those of the bulk metal that it cannot be used. The reason is that tantalum is a good getter, so that the strip becomes strongly contaminated by gas absorption. Preparation of tantalum strips having virtually the same properties as the bulk metal only recently became possible by working at a pressure of about

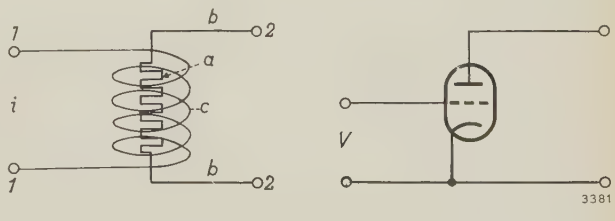

Fig. 5. Making use of the fact that the superconductivity can be removed by the application of a magnetic field, a switching device can be designed whose characteristic resembles that of a triode. An essential difference is that, whereas the triode is driven by a voltage, the device in question (known as a "cryotron") is driven by a current. The figure shows: *a* the superconductor, *b* supply leads and *c* the solenoid providing the magnetic field.

12) The first experiments in this field were done by D. A. Buck, Proc. Inst. Radio Engrs. **44**, 482, 1956.

10^{-11} mm Hg [13]), achieved with a vacuum-pump system of the type recently described in this journal [14]). The use of tantalum is attractive not only because of the favourable situation of its transition point, but also because the vapour-deposited strips are quite hard and of good composition.

It should be emphasized that a superconductor differs essentially from a normal conductor of zero resistance. The fact that a magnetic field penetrates only very superficially into a superconductor is not simply to be explained from the disappearance of the resistance. According to the London-London phenomenological theory, it is necessary in order to describe the behaviour of superconductors to add to the Maxwell equations the expression:

$$\text{curl } \Lambda \mathbf{J}_s = -\mathbf{H}. \quad \ldots\ldots\ldots \quad \text{(II, 1)}$$

Here Λ is a constant, $\mathbf{H}$ the magnetic field, and $\mathbf{J}_s$ the current in the superconductor. For a superconductor this equation takes the place of Ohm's law. If we replace $\mathbf{J}_s$ in (II, 1) by curl $\mathbf{H}$ (in accordance with one of the Maxwell equations), we arrive, after some manipulation, at the equation:

$$\Lambda \nabla^2 \mathbf{H} = \mathbf{H}. \quad \ldots\ldots\ldots \quad \text{(II, 2)}$$

For a superconductor with a plane surface, with $\mathbf{H}$ varying only in the direction perpendicular to that plane, (II, 2) becomes:

$$\frac{\partial^2 \mathbf{H}}{\partial x^2} = \frac{\mathbf{H}}{\Lambda}. \quad \ldots\ldots\ldots \quad \text{(II, 3)}$$

The variation of $\mathbf{H}$ is therefore given by:

$$\mathbf{H}_z(x) = \mathbf{H}_0 \exp(-x/\sqrt{\Lambda}), \quad \ldots\ldots \quad \text{(II, 4)}$$

where $\mathbf{H}_0$ is the value of $\mathbf{H}$ on the surface ($x = 0$). Since the quantity $\sqrt{\Lambda}$, called the penetration depth, amounts to only about 10^{-5} cm, it follows from (II, 4) that the magnetic field scarcely penetrates at all into the superconducting material.

Electron conduction in semiconductors at low temperature

As mentioned in I, the conduction which still occurs in some extrinsic semiconductors when the temperature is so low that there can be no electrons at all in the conduction band, has been attributed to a mechanism called "impurity band conduction", where the electrons are assumed to jump directly from one donor to the other. In this section we shall examine the considerations which led to the discovery of the nature of this remarkable effect — one of the many shown by semiconductors at low temperature. First we shall briefly recall the general experimental method of investigating electron conduction, starting from various theoretical aspects. To begin with the simplest case, we shall return for a moment to metals.

As is well known, electron conduction in metals may be described by the formula:

$$\sigma = ne\mu, \quad \ldots\ldots \quad \text{(II, 5)}$$

where σ is the conductivity, n the concentration of the electrons, e their charge and μ their mobility. The latter quantity is the mean drift velocity of the electrons in unit electrical field, and is related to the mean free path l, the arithmetic mean velocity v of the electrons and the electron mass m, as given by:

$$\mu = el/mv. \quad \ldots\ldots \quad \text{(II, 6)}$$

The conductivity can of course be found directly from the resistance and the geometry. To find the concentration n, and hence indirectly to arrive at the value of μ, use is made of the Hall effect. This effect is a consequence of the force acting on the charge carriers (here electrons) moving in the conductor when it is subjected to a transverse magnetic field. This gives rise to a transverse potential gradient in a direction perpendicular both to the current and to the magnetic field. Between two points on the surface of the conductor, which would otherwise have the same potential, a potential difference is thus measured, whose magnitude V_H in the case of a small bar of rectangular cross-section is given by:

$$V_H = A_H \frac{iH}{d}. \quad \ldots\ldots \quad \text{(II, 7)}$$

Here H is the strength of the magnetic field, i the current, d the thickness of the bar in the direction of H, and A_H is a constant, called the Hall coefficient. It can be shown that A_H is equal to $1/ne$; by determining the value of A_H we can thus find indirectly the value of n.

As stated, (II, 5) and (II, 6) apply only to metals, that is to substances where the mobility is governed entirely by the electrons with energies roughly equal to the Fermi energy. Returning to semiconductors, we see that this condition in their case is not fulfilled. The electron concentration is lower, the energy distribution is often described by Boltzmann statistics instead of by Fermi-Dirac statistics, and it may be necessary to regard the mean free path no longer as a constant but to take into account the way in which it depends on the energy. Having regard to all these considerations, we find that A_H still satisfies an equation of the above-mentioned form, but that a numerical factor f must be added, the value of which — between 1 and 2 — may differ somewhat depending on the circumstances. It is evident that,

---

[13]) J. F. Marchand and A. Venema, Philips Res. Repts. **14**, 427, 1959.

[14]) A. Venema and M. Bandringa, Philips tech. Rev. **20**, 145, 1958/59.

in order properly to interpret a measurement of the Hall effect, reliable assumptions are needed regarding the mechanism by which the electrons are scattered and regarding the statistics to be applied.

To approach a little closer to our goal, we shall now consider what changes the Hall effect may undergo where two conduction mechanisms are responsible for the motions of the electrons. It is then as if two currents were flowing in the semiconductor. The electrons of the one current possess the mobility μ_1, those of the other the mobility μ_2. The manner in which the total electron concentration n is built up from the fractions n_1 and n_2, corresponding to the two currents, will depend on the temperature. (The value of n itself is also temperature-dependent, but that is not relevant for our present purposes.) We may express the above mathematically as follows:

$$\sigma = \sigma_1 + \sigma_2 = n_1 e\mu_1 + n_2 e\mu_2 \quad . \quad . \quad \text{(II, 8)}$$

and

$$n_1/n_2 = a(T). \quad . \quad . \quad . \quad . \quad . \quad \text{(II, 9)}$$

The densities of the two component currents are:

$$i_1 = \frac{\sigma_1}{\sigma_1 + \sigma_2} i \quad \text{and} \quad i_2 = \frac{\sigma_2}{\sigma_1 + \sigma_2} i.$$

It can be calculated that the Hall coefficient in this case is given by:

$$A_H = \frac{\sigma_1\mu_1 + \sigma_2\mu_2}{(\sigma_1 + \sigma_2)^2}. \quad . \quad . \quad \text{(II, 10)}$$

Putting $\mu_1/\mu_2 = b$, we can write (II, 10) as:

$$A_H = \frac{1}{(n_1 + n_2)e} \frac{(ab^2 + 1)(a + 1)}{(ab + 1)^2} \quad . \quad \text{(II, 11)}$$

$$= \frac{1}{ne} f(a,b). \quad . \quad . \quad . \quad \text{(II, 12)}$$

The variation of A_H with temperature is thus determined by the way in which n and $f(a,b)$ vary with temperature. Now, n is of course a monotonic function of T, but $f(a,b)$ is not. At a certain temperature the latter function shows a maximum, and consequently the same holds for A_H; where a combination of conduction mechanisms occurs as in the model just described, the Hall coefficient in a particular temperature range may often be appreciably larger than outside that range.

If we assume that b is not temperature-dependent, it follows from (II, 11) that the maximum value of $f(a,b)$ is equal to $(b + 1)^2/4b$. The temperature at which this maximum occurs is then governed only by the way in which $a = n_1/n_2$ varies with temperature.

This remarkable behaviour of A_H has indeed been found in certain cases, including germanium [15]) and cadmium sulphide [16]). The impossibility of explaining this behaviour with any other model gave rise to the hypothesis that two conduction mechanisms must be operative in these semiconductors. In germanium the maximum value of A_H was found in a particular case to be about 100 times greater than the values found at higher and lower temperatures. From considerations that cannot be discussed here (see reference [16])), and the fact that the second mechanism, although characterized by a small electron mobility, makes a relatively large contribution to the current in the temperature range where the conduction band is virtually empty, it was concluded that this mechanism must be that understood by "impurity band conduction".

---

[15]) C. S. Hung, Phys. Rev. **79**, 727, 1950.
[16]) F. A. Kröger, H. J. Vink and J. Volger, Philips Res. Repts. **10**, 39, 1955.

Summary. The residual resistance shown by a metal at extremely low temperature is due to the scattering of the electrons by lattice imperfections. Plastic-deformation experiments on highly purified aluminium give a picture of the individual influence of point defects and dislocations. The magnetoresistance of copper is found to obey Kohler's rule only in so far as the residual resistance is due to point defects in the lattice: dislocations cause a deviation from this rule. The residual resistance of iron contaminated with carbon is proportional to the carbon concentration but not entirely independent of temperature (as it should be to obey Matthiessen's rule). The fact that the superconducting transition temperature depends on an external magnetic field is turned to use in a switching element made of vapour-deposited tantalum. In some extrinsic semiconductors, conduction occurs at low temperature as a result of the mechanism whereby the electrons jump directly from one donor to the other (impurity band conduction).

A MAGNETIC JOURNAL BEARING

by F. T. BACKERS.

621.822.824:538.12:621.318.124

The supporting of a rotating shaft in such a way that no material contact is made with the shaft can be of importance for technical applications. Cases in point are where the friction or wear must be particularly small, where contamination by lubricants is inadmissible or where the lubricating oil would decompose under the influence of radiation (in a nuclear reactor, for example). The article below considers the theory of a shaft which is held in suspension by magnetic fields, and compares the theory with the results of measurements which have been made on "magnetic bearings" of various dimensions.

Rotating shafts are supported by bearings, and the necessary reactions are provided by material contact between shaft and bearing. The friction and wear which are the unavoidable consequence of this contact, are limited as much as possible by using lubricants.

The idea of reducing the friction and wear to nil by making the shaft "float" is attractive. One approach to this problem is based on levitation by the application of magnetic fields [1]). Those methods which rely on the use of a diamagnetic body or of a superconductor [1]) are for practical reasons not very useful. Also methods in which the supporting force comes from electromagnets are open to the objection that a continuous supply of energy is necessary for levitation. The only remaining alternative possibility, using permanent magnets to provide the support, has been described in a patent application [2]) but, as far as we know, has never been realized. In the Philips laboratory at Eindhoven, a study has been made of such magnetic bearings. A number have been constructed and measurements on them have verified the theory.

Description of the magnetic bearing

The principle of the magnetic bearing considered here is illustrated in *fig. 1*. On the shaft A are fixed a number of radially magnetized rings B, made of the ceramic permanent-magnet material ferroxdure I. Adjacent rings have opposite polarity: if the magnetization in the p^{th} ring is directed *towards* the shaft, the magnetization in the $(p-1)^{\text{th}}$ ring and the $(p+1)^{\text{th}}$ ring is directed *away* from the shaft. In fig. 1, each of the two bearings has four of these shaft rings. A greater number can also be used; the theory is based upon an extremely large number.

The shaft, with its rings B, is placed in the field of a like number of larger rings C of the same thickness, which are fixed in the bearing housing. These C rings are also made of ferroxdure I and have alternate polarities which, however, are opposed to those of the corresponding shaft rings. That the resulting *radial* equilibrium is stable is seen from the following. When, as a result of external forces upon the shaft, the concentricity of the rings B and C is disturbed, the magnetic force at the place where the rings are closest is always larger than that at the diametrically opposite position. If each shaft ring is of opposite polarity to the corresponding outer ring, the resulting force tends to return the shaft towards the concentric position. Thus, as far as radial deviations are concerned, the shaft is in stable equilibrium. If opposing shaft and outer rings had the same polarity, there would still be an equilibrium possible, but it would be unstable.

During an *axial* deviation, a force develops which tends to make the deviation still greater, so that in an axial direction the equilibrium is unstable. This is in accordance with a theorem due to Earnshaw [3]), which can be formulated in the following way: a permanent magnet placed in the field of other permanent magnets cannot remain in stable equilibrium. However, the axial instability can be kept within bounds by letting the shaft abut a stop when the deviation reaches a certain value. Another method, in which material contact is excluded, will be discussed later (see Notes, *c*, page 237).

The theory will show that it is better to construct a bearing from a number of adjacent rings of opposed polarities instead of from one ring having the same polarity throughout.

---

[1]) A. H. Boerdijk, Levitation by static magnetic fields, Philips tech. Rev. **18**, 125-127, 1956/57.

[2]) German Patent Application B 30 042 dated 1954 (German Specification 1 017 871 dated 1957) by M. Baermann.

[3]) S. Earnshaw, Trans. Cambr. Phil. Soc. **7**, 97-112, 1842. See also: J. C. Maxwell, A treatise on electricity and magnetism Clarendon, Oxford 1873, Part 1, pp. 139-141.

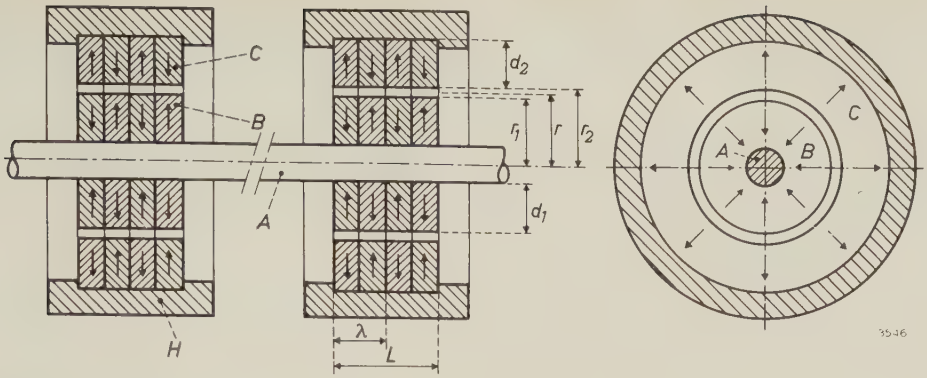

Fig. 1. Diagram showing the principle of a shaft with two magnetic bearings. The inner rings B are fixed on the shaft A. This assembly can rotate in the field of the stationary outer rings C. All the rings are magnetized radially. Adjacent rings are magnetized in opposite directions; likewise corresponding inner and outer rings. H housing.

The theory of the magnetic bearing

In the magnetic bearing, two characteristic quantities occur: the radial carrying capacity F_0, being the external force upon the shaft which is necessary to bring the shaft rings into contact with the outer rings; and the radial stiffness S, denoting the force per unit displacement in a radial direction. These two quantities are calculated below.

We consider an infinitely large flat plate C of ferroxdure having a thickness d (*fig. 2*). The plate is so orientated in the system of coordinates shown

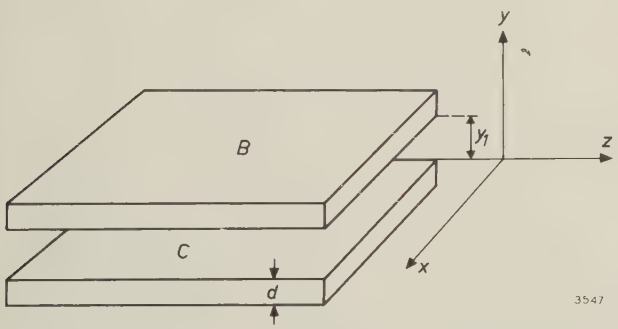

Fig. 2. Two plates B and C regarded as being infinitely large, both magnetized in the y direction. The magnetization of plate C is $I = I_0 \cos 2\pi z/\lambda$ and that of plate B is $I = I_0 \cos 2\pi(z + z_0)/\lambda$.

that the upper surface lies in the plane $y=0$. The plate is magnetized in the y direction, the strength of the magnetization I ($= B - \mu_0 H$) being solely a function of z and, as we will assume for the moment, a cosine function:

$$I = I_0 \cos 2\pi z/\lambda .$$

This expression defines a periodically recurring distance λ (the "wavelength") in the z direction. Later, we shall consider the case when I is another function of z.

An important quantity is the magnetic potential, i.e. the quantity from which the components H_x, H_y and H_z of the magnetic field are obtained by differentiating with respect to x, y and z respectively. The magnetic potential U at a point (x,y,z) above the plate can be calculated, albeit not simply, by means of the formula:

$$U(x,y,z) = \frac{1}{4\pi\mu_0} \int_V \frac{\mathbf{I}\cdot\mathbf{r}}{r^3}\, \mathrm{d}V .$$

Here, μ_0 is the permeability of free space (equal to $4\pi \times 10^{-7}$ H/m), $\mathbf{r}$ the radius vector of the volume element $\mathrm{d}V$ at the point (x,y,z), and $\mathbf{I}$ the magnetization vector. Integration over the volume of the plate yields:

$$U(x,y,z) = \frac{I_0\lambda}{4\pi\mu_0} \{1 - \exp(-2\pi d/\lambda)\} \{\exp(-2\pi y/\lambda)\} \cos 2\pi z/\lambda .$$

By differentiation, the y component of the magnetic field-strength is given by: $H_y = -\partial U/\partial y$.

Let B be a second plate of ferroxdure parallel to the plate C at a distance y_1 away from it (fig. 2). The plates B and C are assumed to be identical, except that the magnetization of B is spatially displaced in phase with respect to that of C:

$$I = I_0 \cos 2\pi(z + z_0)/\lambda .$$

The potential energy of B in the field of C is now:

$$E = -\int_V \mathbf{I}\cdot\mathbf{H}\, \mathrm{d}V = -\int_V I\, H_y\, \mathrm{d}V ,$$

where the vector $\mathbf{I}$ is the magnetization of the plate B and the vector $\mathbf{H}$ the field of the plate C. If we write $E(\lambda,w)$ to denote the energy of an element of plate B of length λ in the z direction, of breadth w in the x direction and of thickness d, then the repul-

sive force to which B is subjected in the field of C is, per unit area:

$$\sigma_y = -\frac{1}{w\lambda}\frac{\partial E(\lambda,w)}{\partial y}.$$

In this way it is found that:

$$\sigma_y = -\frac{I_0^2}{4\mu_0}\{1-\exp(-2\pi d/\lambda)\}^2 \{\exp(-2\pi y_1/\lambda)\}\cos 2\pi z_0/\lambda.$$

If only λ is varied in this expression, it appears that σ_y approaches zero in the two limiting cases $\lambda \to 0$ and $\lambda \to \infty$. In the first case, the opposed polarities approach infinitely closely to one another so that they neutralize each other's effect. In the second case, the magnetic field is contained totally within the ferroxdure and there is thus no external field present; this can be seen when it is realized that H in the infinitely large plate must be constant (lines of force parallel) and can therefore only have the value zero, since the lines of force outside the plate are infinitely long. The existence of two limiting cases suggests that somewhere in between there should be an optimum value of λ.

Since σ_y is positive in the direction of the positive y axis, a maximum *attractive* force will be obtained when the phase displacement z_0 is equal to zero, i.e. the magnetization of plate B is spatially in phase with that of C (this can be seen by inspection). Since, in the case of the magnetic bearing, a maximum *repulsive* force is required, z_0 is chosen equal to $\frac{1}{2}\lambda$; the magnetization of B is then displaced by a half wavelength from that of C. Again, the thickness d is assumed to be sufficiently large in order to make $\exp(-2\pi d/\lambda)$ negligible with respect to unity; $d = \lambda$, for example, makes this term approximately 0.002. These considerations lead to:

$$\sigma_y = \frac{I_0^2}{4\mu_0}\exp(-2\pi y_1/\lambda). \quad . . . \quad (1)$$

In order to transform the flat plates B and C into the bearing, we cut pieces of suitable dimensions out of the plates and bend these pieces into the form of hollow cylinders, the axes of which are parallel with the z axis and whose radial direction corresponds to the original y direction. The distance y_1 is now represented by the distance between the shaft rings B and the outer rings C of the bearing described earlier, and the length (dimension in axial direction) of a ring is $\frac{1}{2}\lambda$. It is assumed throughout that the repulsive force, acting upon an element of B, predominantly emanates from a limited area of C in the immediate vicinity of that element of B. If the radius of curvature of the cylinder is large compared with y_1, then this small area of C can be regarded as flat. The above theory for the "flat case" can then be applied to the cylindrical case, i.e. that of the bearing.

The radial force acting upon a surface element $Lr\,d\Theta$, where L is the length of the bearing and r the mean radius (fig. 1), is now:

$$dF_y = \sigma_y\, Lr\, d\Theta. \quad . . . . . \quad (2)$$

Here, σ_y is given by (1); the y_1 which occurs in (1) can be approximated (see *fig. 3*) by

$$y_1 = c + e\cos\Theta, \quad . . . . . \quad (3)$$

where e is the eccentricity of the shaft and c its *maximum* radial displacement which is equivalent to the difference of the radii of the opposing surfaces of the rings — in the following called the "clearance". The angle Θ is measured in fig. 3 from the point where y_1 is a maximum.

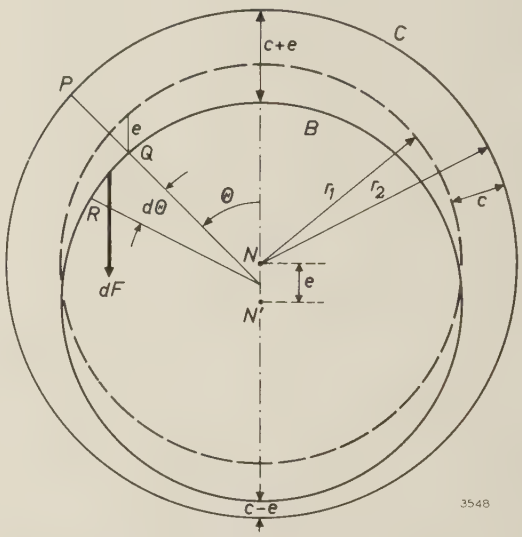

Fig. 3. Shaft eccentric with respect to bearing. N is the centre of the outer rings, N' the centre of the inner rings. The eccentricity is e. In the concentric position (dashed line) N' coincides with N. If r_1 does not differ greatly from r_2, then, approximately:

$$y_1 = PQ = c + e\cos\Theta \text{ and } RQ = r\,d\Theta,$$

where r is the average of r_1 and r_2. dF is the component of the force acting upon the element $rL\,d\Theta$, parallel to the displacement.

From considerations of symmetry it can be seen that, upon radial displacement, the resulting force cannot have any component perpendicular to the displacement. The contribution which the force acting on the element $Lrd\Theta$ makes to the total restoring force, opposing the displacement, is therefore:

$$dF = -\cos\Theta\, dF_y. \quad . . . . . \quad (4)$$

Thus, for $-\frac{1}{2}\pi < \Theta < \frac{1}{2}\pi$ this contribution is negative, in other words it tends to increase the displacement, while the part of the bearing for which $\frac{1}{2}\pi < \Theta < \frac{3}{2}\pi$ makes a positive contribution. After

integrating equation (4) over Θ, and substituting from equations (1), (2) and (3), the total restoring force F is found, this force being a maximum when the eccentricity e is equal to the clearance c, and being then equivalent to the radial carrying capacity F_0 which was what we set out to calculate. We now have:

$$F = -A \exp(-b) \int_0^{\pi} \cos\Theta \exp(-b' \cos\Theta)\, d\Theta,$$

where $A = LrI_0^2/2\mu_0$, $b = 2\pi c/\lambda$ and $b' = 2\pi e/\lambda$. The maximum value of F, i.e. the radial carrying capacity F_0, follows immediately by putting $b' = b$, i.e. $c = e$.

From a numerical calculation of F_0 as a function of b, it appears that F_0 has a fairly flat maximum for values of b in the neighbourhood of 1. From this it follows that the relation

$$b = 2\pi c/\lambda = 1 \quad . \ . \ . \ . \ . \quad (5a)$$

defines an optimally dimensioned bearing. The axial length $\frac{1}{2}\lambda$ of each ring should thus be approximately three times the clearance c. The magnitude of the carrying capacity is then 0.655 A, i.e.

$$(F_0)_{max} = 0.655\, LrI_0^2/2\mu_0. \quad . \ . \quad (5b)$$

In *fig. 4* the restoring force F, as a percentage of $(F_0)_{max}$, is reproduced as a function of b' for various values of b. These curves represent the bearing characteristics. For values of b approximately equal to 1 the characteristic is virtually linear, so that the radial stiffness S can be represented by:

$$S = (F_0)_{max}/c.$$

In the above, it is assumed that the magnetization varies according to a cosine function. The calculation can also be carried out for a discontinuously changing radial magnetization, i.e. for a square waveform:

$$I = +I_0 \text{ for } 0 < z < \tfrac{1}{2}\lambda,$$
$$I = -I_0 \text{ for } \tfrac{1}{2}\lambda < z < \lambda, \text{ and so on.}$$

In this case, the maximum carrying capacity is:

$$(F_0)_{max} = 1.20\, LrI_0^2/2\mu_0, \quad . \ . \ . \quad (6)$$

in other words, about 1.8 times as large as in the case of (5b).

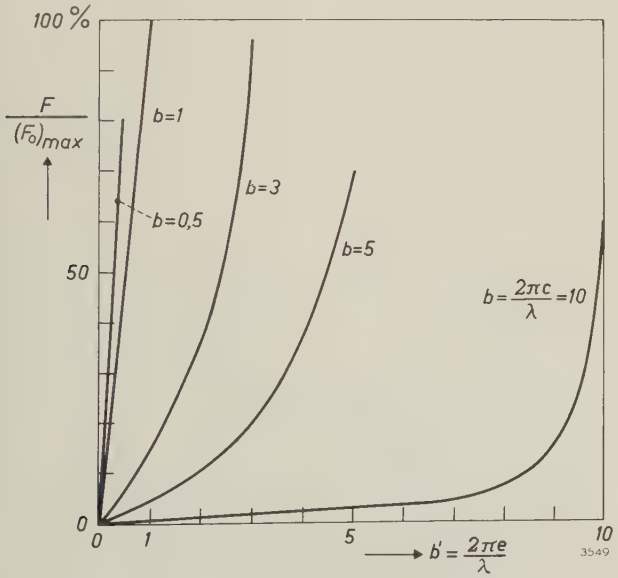

Fig. 4. Calculated bearing characteristics where the magnetization is assumed to vary according to a cosine function. The force F (restoring force towards the concentric position) is represented as a percentage of the carrying capacity $(F_0)_{max}$ and reproduced as a function of the eccentricity e for values of the parameter b ($= 2\pi c/\lambda$). For a given b, the largest possible value of F is attained when e is equal to the radial clearance c, i.e. when $b' = b$. In that case F represents the load capacity F_0 of the bearing. The most favourable value of b is unity, this giving a maximum value for F_0.

Experimental results

A bearing was made in which λ and c could be varied, with a view to testing certain theoretical relationships. The fact that $b = 2\pi c/\lambda$ should optimally be equal to about 1 can easily be tested, there being no difficulty in measuring c and λ. It is not so simple to check $(F_0)_{max}$, however, since to do so we must know the magnitude of I_0, which is not easy to measure with the required accuracy. Furthermore, it is necessary to know the "type" of magnetization, e.g. whether it varies as a cosine or a square wave function. And lastly there is the question of whether I_0 is constant in the ferroxdure in a radial direction. Plainly, then, the experiments can do no more than give a rough check of the formula for the carrying capacity.

Three types of rings were made (80 of each type), comprising one type of outer ring C and two types of shaft rings B and B' (*fig. 5*). At both ends of a shaft, which also carried a wheel, 40 shaft rings were mounted; two groups of outer rings C, each consisting of 40 rings, formed the fixed part of the bearings. The axial length of the rings is 1.5 mm; this defines the

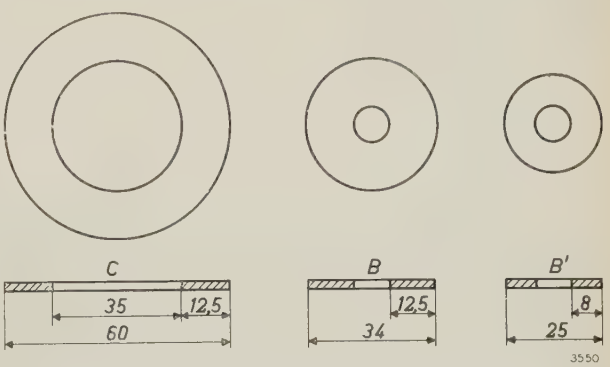

Fig. 5. Dimensions of the outer ring C and two kinds of shaft rings B and B' used in the tests.

minimum value of $\frac{1}{2}\lambda$. If n rings of like polarity are placed together, then $\frac{1}{2}\lambda = n \times 1.5$ mm.

The following combinations of rings were tried:

1) Rings C and B with alternate polarity, so that $\lambda = 3$ mm. The dimensions of the rings are such that the clearance c is 0.5 mm, from which it follows that b $(= 2\pi c/\lambda)$ is ~ 1.
2) Rings C and B in batches of ten adjacent rings of like polarity: $\lambda = 30$ mm, $b \approx 0.1$.
3) Rings C and B'. The B' rings are of smaller diameter than the B rings, such that $c = 5$ mm. Here, λ is again 3 mm, so that b is ~ 10.

In the experiments (1) and (2) the radius r was about $17\frac{1}{2}$ mm; in all three cases the combined length of the two bearings was $L = 120$ mm.

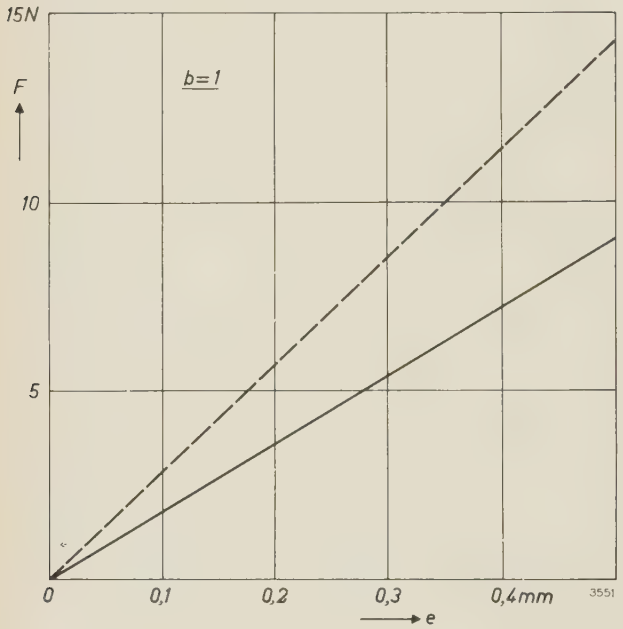

Fig. 6. Characteristic of an optimally dimensioned bearing ($b = 1$). The dashed characteristic was calculated for sinusoidal magnetization with $I_0 = 0.17$ Wb/m². The full line is the measured characteristic.

The characteristics of the three types of bearings (force F in newtons as a function of the eccentricity e in mm) are given in *figs. 6, 7, 8* and *9*; the full curves represent the experimental results and the dashed curves the calculated values. In fig. 9 particularly, it is clear that the radial carrying capacity and the radial stiffness are greatest for $b = 1$.

As far as the type of magnetization is concerned, a good approximation to a square form can be expected in case (2), where λ is large, whilst in the cases (1) and (3) a cosine function would approximate more closely to the actual form. For case (2), fig. 7, the theoretical curves for both types of magnetization are given.

In the case of the rings B and C the radial thickness d is approximately 12.5 mm and in the case of rings

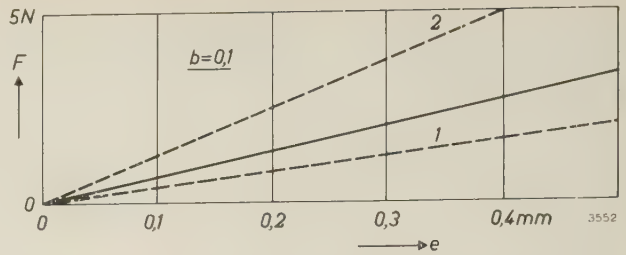

Fig. 7. Characteristic of bearing where $b = 0.1$. The dashed lines *1* and *2* are calculated characteristics with $I_0 = 0.17$ Wb/m² (*1* for sinusoidal magnetization, *2* for discontinuously changing magnetization). The full line is the measured characteristic.

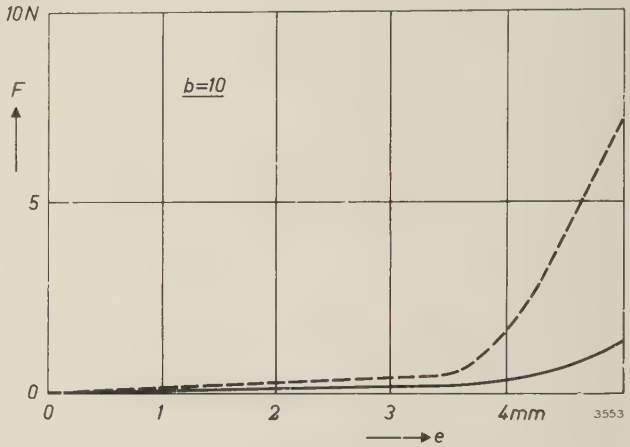

Fig. 8. Characteristic of a bearing where $b = 10$. The dashed line is the calculated characteristic for sinusoidal magnetization with $I_0 = 0.17$ Wb/m². The full line is the measured characteristic.

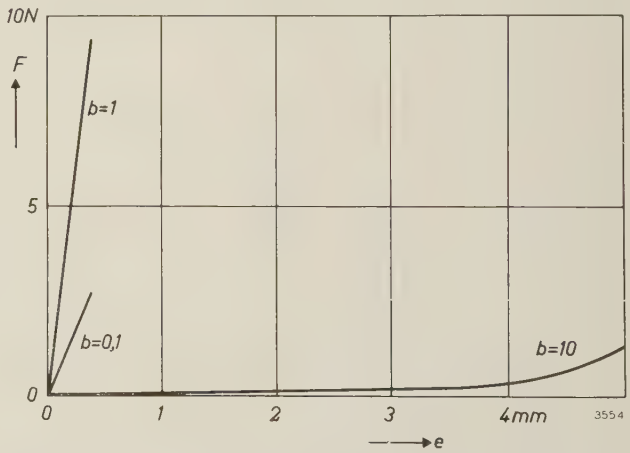

Fig. 9. The three measured bearing characteristics in one diagram. The bearing is optimally dimensioned when $b = 1$.

B' approximately 8 mm. It follows from this that we are amply justified in neglecting $\exp(-2\pi d/\lambda)$ with respect to unity in the cases (1) and (3), but not in case (2), where d is approximately $\frac{1}{2}\lambda$ and $\exp(-2\pi \times 12.5/30) \approx 0.07$. In the calculation for case (2) the term $\exp(-2\pi d/\lambda)$ is therefore not neglected.

If we now compare the theoretical and the measured characteristics with each other, we see first of all that in case (3), fig. 8, the divergence between the theoretical and the measured value of F_0 is very considerable. This is not surprising, since the theory

supposes the clearance c to be small compared with the average radius r, and this requirement is not fulfilled here. On the other hand, in cases (1) and (2), it appears that the differences between the theoretical and the measured curves are probably due to an error in the measurement of the magnetization. The latter was measured in various ways. The average of the measurements was: $I_0 = 0.17$ Wb/m^2 with a possible error of approximately 20%. Since $(F_0)_{max}$ is proportional to I_0^2, this error can lead to one of approximately 40% in the final result. Assuming that the theory is correct and that in case (1) the magnetization followed a cosine function, it follows from the measured curve in fig. 6 that: $I_0 = 0.13$ Wb/m^2. This value does not deviate more than about 20% from the average measured value. If we choose this "corrected" value for calculating the theoretical curves in case (2), fig. 7, then the curve for a discontinuously changing magnetization more or less coincides with the measured curve.

It should be added that the measurements of I_0 are, in fact, measurements of the remanence or residual magnetization. This is only equal to the magnetization in the present situation (magnet in the field of another magnet) if the relative permeability μ_r is equal to 1, since an external field H increases the magnetization by the amount $\mu_0(\mu_r - 1)H$, which is zero only when μ_r is unity. This is approximately so in the case of ferroxdure, and therefore it may be assumed that the measurements give the approximate magnetization of the ferroxdure in the assembled bearing.

Another practical advantage of ferroxdure is its high electrical resistivity, so that very low eddy-current losses occur during the rotation of the shaft.

Notes

a) Both the weight of the shaft ring and $(F_0)_{max}$ increase linearly with the length L; however, as the radius r of the bearing is increased, the weight increases quadratically whilst $(F_0)_{max}$ increases only linearly. Now, in order to avoid using up the whole radial carrying capacity to maintain the weight of the shaft itself in the case of large horizontal shaft assemblies, we make use of the fact that although the radial thickness d must be large enough (compared to λ), it does not have to be so much larger than λ. It is therefore possible to make use of hollow shafts of large diameter, fitted with rings of relatively small radial thickness. In this way, advantage is taken of the linear increase of $(F_0)_{max}$ with respect to r, while the weight now increases much less than proportionally to the square of r.

With the types of bearing used in our experiments, the weight of the shaft complete with rings and wheel was just under 1 kg, i.e. almost as much as the carrying capacity of the bearing with optimum clearance ($b = 1$, fig. 6). By means of the measures just mentioned, the design can be improved to fulfil practical requirements. Again, a better material can be used (see the following note).

b) In the foregoing we have been concerned solely with radially oriented magnetization. The same formulae also apply, however, to axial magnetization of the same rings, although this will not be further amplified here. One advantage of axial magnetization is that the direction of I is the same throughout each ring, making it possible to use crystal-oriented ferroxdure II, which has a higher remanence [4]); this is a great advantage since $(F_0)_{max}$ is proportional to I_0^2. The preferred direction of magnetization in the ferroxdure II should then coincide with the axial direction of the rings.

c) It is assumed that the shaft and outer rings are directly opposite each other (see theory; $z_0 = \frac{1}{2}\lambda$). If this is not the case, the carrying capacity must be multiplied by $\cos 2\pi z_0/\lambda$, which indicates that

[4]) A. L. Stuijts, G. W. Rathenau and G. H. Weber, Ferroxdure II and III, anisotropic permanent magnet materials, Philips tech. Rev. **16**, 141-147, 1954/55.

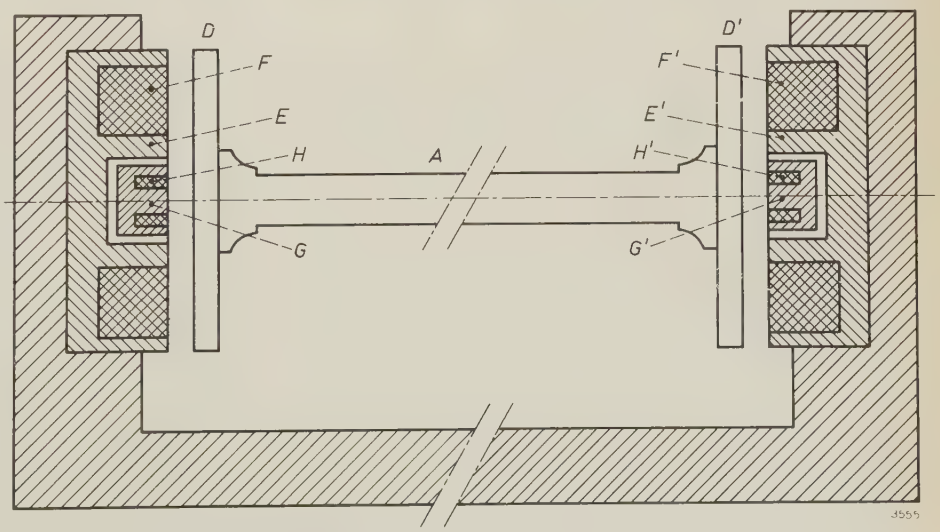

Fig. 10. System for stabilizing the shaft in an axial direction. D and D' are ferroxcube disks which can be attracted by electromagnets E and E', excited by coils F and F'. The self-inductance of the coils H and H' on the cores G and G' is dependent upon the distance to the disks D and D'. The magnetic bearings themselves are omitted here.

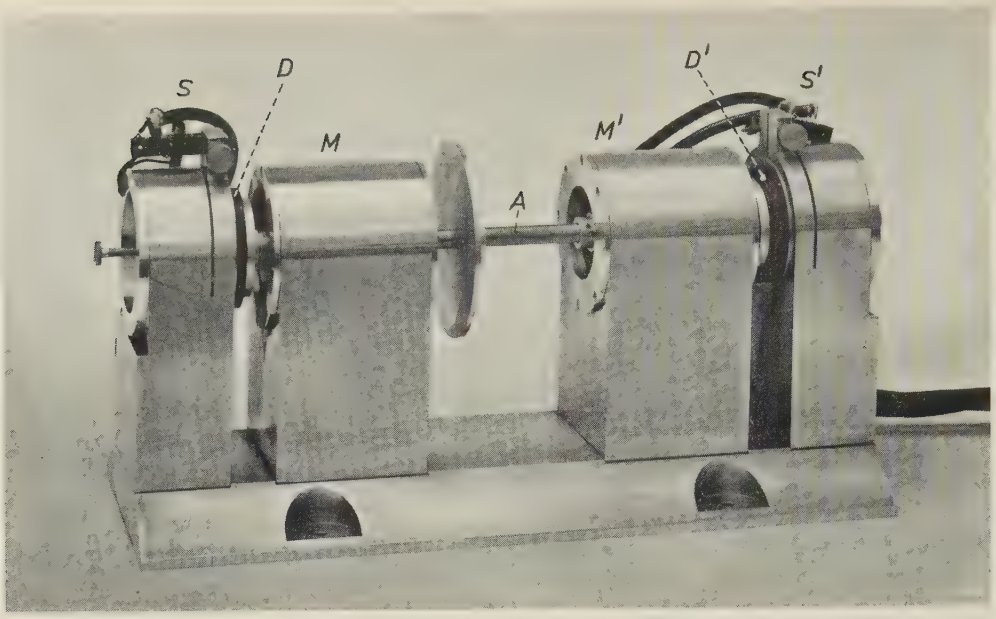

Fig. 11. Shaft A with magnetic bearings M and M', ferroxcube disks D and D' and axial stabilizers S and S'.

good positioning in the axial direction is important, especially when λ is small. A method has been developed for locating the shaft in an axial direction without material contact. Use is made of an electro-mechanical servo-mechanism, the principle of which can be seen in *fig. 10* (the bearing itself being excluded). A photograph of the whole bearing with servo-mechanism is shown in *fig. 11*. D and D' are disks of ferroxcube, E and E' are electromagnets excited by coils F and F', while H and H' are coils having cores G and G'. The self-inductance of each of the coils H and H' decreases as the distance to its opposing disk increases, which makes it possible to electrically "measure" the axial position of the shaft. H and H' form two arms of a bridge circuit (*fig. 12*); an error in the position of the shaft disturbs the balance of the bridge. Depending on the direction of displacement of the shaft from the central position, a phase-sensitive detector D energizes the coil F or F' in such a way that the shaft is drawn back to the equilibrium position. A suitable network (not drawn) between the detector and the coils F and F' provides the necessary stability in the servo-system.

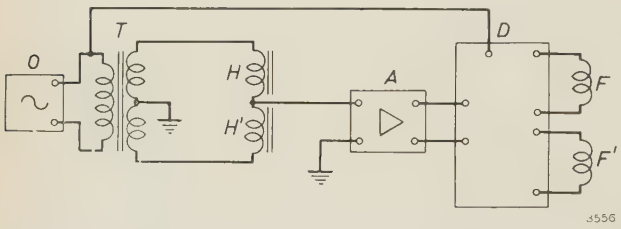

Fig. 12. The coils H and H' (fig. 10) form two arms of a bridge circuit which is fed via a transformer T by an oscillator O. When the self-inductance of H is equal to that of H', the bridge is in balance. An axial displacement of the shaft unbalances the bridge; this causes the phase-sensitive detector D to energize whichever of the coils F and F' is required to bring the shaft back to the central position. A amplifier.

Summary. Bearing wear and friction of a rotating shaft can be avoided by avoiding all material contact between shaft and bearing. This may be done by letting the shaft "float" in a magnetostatic field. For this purpose "magnetic bearings" have been constructed, consisting of ring magnets fixed to the shaft situated within a set of outer stationary ring magnets. The rings consist of ferroxdure I and are radially magnetized. The direction of magnetization of adjacent rings is alternately directed towards and away from the shaft, and opposing inner and outer rings have mutually opposed directions of magnetization. In an axial direction, the alternating direction of magnetization defines a "wavelength" λ. It is found theoretically that the bearing is optimally dimensioned when the clearance between the inner and outer rings is equal to $\lambda/2\pi$; experiments confirm this result. The bearing is stable in a radial direction; it is stabilized in an axial direction by a simple electromechanical servo-system.

VISUAL INSPECTION OF MOVING LAMP FILAMENTS ON A COILING MACHINE

by F. EINRAMHOF *).

621.397.331.2:621.326.032.321

In the mechanical production of coiled filaments for incandescent lamps the quality of the coils must be regularly inspected. It is not necessary to examine each coil separately, a sampling inspection being sufficient. The number of samples to be taken is quite considerable, however, for example about 1 in 30. Since the primary object of the inspection is to ensure that the machine is properly lined up and that the wire used is of good quality, the coil should preferably be examined immediately after it has been wound, i.e. before it is cut into separate filaments. This means that either the coils must be observed while they are moving, or the machine must be stopped for a moment for each inspection. The latter is obviously undesirable, and so the coils are examined in motion. In view of the minute details involved, a microscope is indispensable for this purpose.

Until recently the time taken by one coil to traverse the field of view of the microscope was long enough for a reliable appraisal. The latest coiling machines work so fast, however, that this is no longer the case. It was therefore necessary to find some means of artificially extending the observation time without depriving the inspection of its instantaneous character. This can be done in several ways. The choice ultimately fell on a method using closed-circuit television equipment. The principle will be illustrated with reference to *fig. 1*.

On the left the coil *1*, still on the mandrel, can be illuminated by a flash-tube *2* (circular or U-shaped) and a cylindrical mirror *3*. The microscope *4* is focused on the coil. Behind the microscope is mounted a television camera *6*, focused on infinity and connected via a power supply and control circuit *7* to a television receiver *8*. The cathode-ray tube screen is shielded from daylight by a visor *9* and is fitted with a yellow filter *10*. The observer presses a push-button switch *11* to actuate the circuit *12* for triggering the flash-tube. There then appears on the screen a picture of the coil which is under the microscope at the moment of the flash. In the absence of a flash, the picture tube is biased just below the threshold of illumination.

The picture remains visible for about 30 seconds,

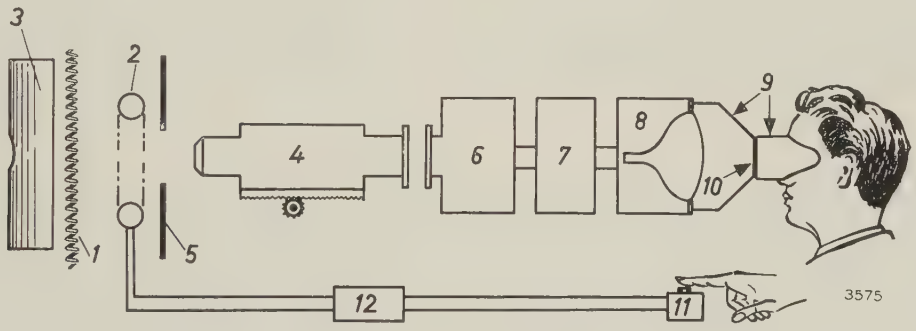

Fig. 1. Block-diagram of set-up for inspecting lamp filaments on the point of leaving the coiling machine. *1* coil on winding mandrel (not shown). *2* flash-tube (duration of flash 10 μsec). *3* mirror for concentrating the illumination. *4* microscope, focused on *1*. *5* screen preventing direct incidence of light on microscope objective (for the same reason the mirror has a hole in the middle). *6* vidicon television camera and pre-amplifier. *7* electronic circuit for power supply and vidicon control. *8* television receiver with long-persistence screen (30 sec afterglow). *9* visor to shield the screen from daylight. *10* yellow filter. *11* switch for actuating the flash-tube triggering circuit *12*.

and it is bright enough during the first 10 to 15 seconds to be closely examined. On the other hand the light-flash is short enough to preclude movement blur. These advantages are due to the following features of the set-up. In the first place, the television camera is equipped with a vidicon, i.e. a photoconductive camera tube [1]). Owing to the slow decay of the charge pattern produced in the photoconduct-

*) Philips Lighting Division, Eindhoven.

[1]) P. K. Weimer, S. V. Forgue and R. R. Goodrich, R. C. A. Rev. **12**, 306, 1951. See also: L. Heijne, P. Schagen and H. Bruining, Philips tech. Rev. **16**, 23, 1954/55.

ing layer upon exposure, scanning is possible in the normal time of 1/25th sec. The flash does not have to be synchronized with the movement of the scanning beam, the position of the beam at the moment of the flash being unimportant. The extension of the observation time to the duration mentioned above is due to the use of a cathode-ray tube screen having an exceptionally long afterglow. This screen — a normal radar type — consists of two luminophor layers, one fluorescent and the other phosphorescent. The first is exicted into blue fluorescence by the electron beam. The second, excited by the light from the first, emits yellow light, which persists for a time after the fluorescence has ceased. It will now be clear why the observer looks at the screen through a yellow filter: the short-lived but intense blue light would otherwise dazzle him, making further observation very difficult.

Now a word about the illumination of the object. With a suitable flash-tube, the duration of the flash can be varied from a few microseconds to a few milliseconds by varying the inductance in the flash-tube circuit. If we choose a flash duration of 10 μsec, for example, and allow a movement blur of 0.5 mm on the screen — a better definition would be pointless — an object reproduced at its true size may then admissibly travel at a speed of up to 50 metres per second, or 180 km/h. Where a magnification of × 100 is required, as it is for the inspection of coiled filaments, the maximum permissible speed of the

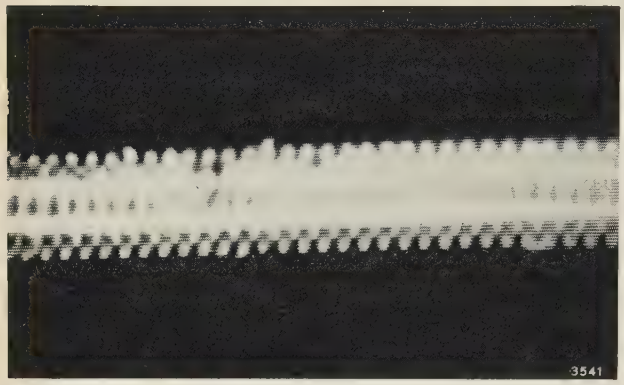

a

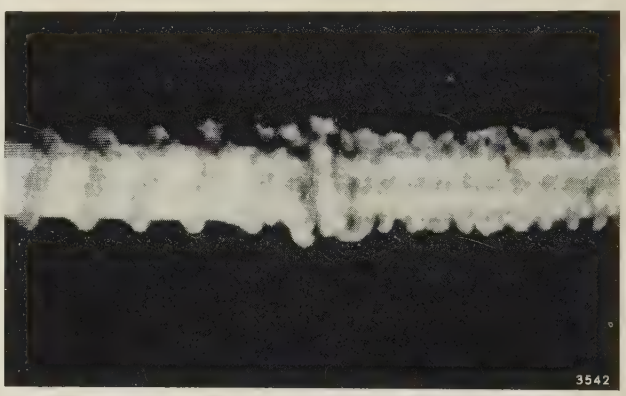

b

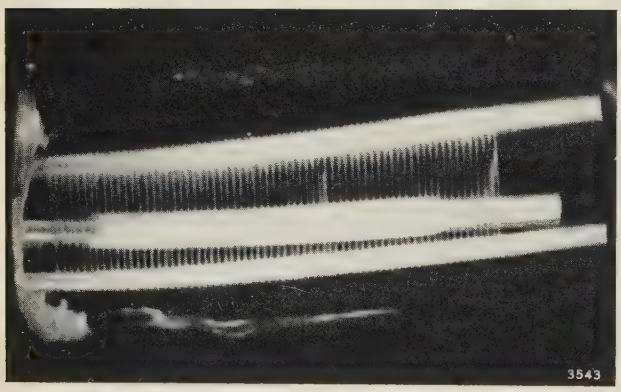

c

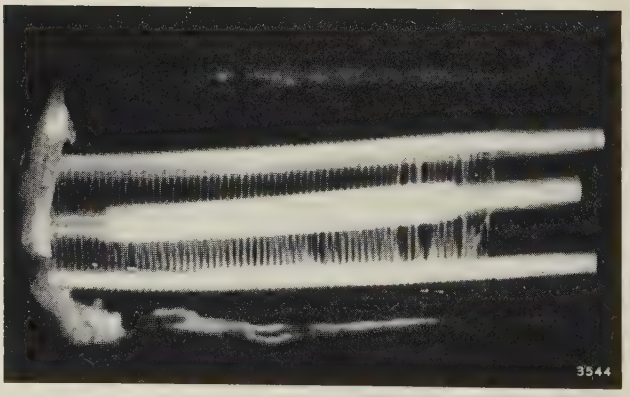

d

e

Fig. 2. Photographs of pictures obtained on the television screen with the set-up of fig. 1. The magnifications mentioned refer to the equipment itself; the figures reproduced here are about 6 × smaller than on the screen. *a*) Good coil (× 100). *b*) Faulty coil (× 100). To illustrate the application of the method to other processes, the following two photographs show the cathode and the first grid of a radio valve, *c*) undamaged and *d*) damaged. The chance of damage here is not in the winding process but in the mechanical mounting of the finished grid around the cathode. The magnification in this case is only × 6. The extent to which movement blur is reduced by the illumination of only 10 μsec appears from *e*). Although the tips of the fan blades shown are revolving at about 180 km/h, there is no perceptible blur.

object must be 100 times smaller, i.e. 50 centimetres per second. This is still quite a considerable speed.

The illumination of the object must obviously not be so intense as to overload the vidicon and to risk overdriving the amplifier behind it. A wide range of illumination intensities can be covered, however, if an iris diaphragm is incorporated in the optical system and the amplifier suitably adjusted.

It will be evident that the method described here can be used for examining all kinds of other rapid transients (periodic processes can best be observed stroboscopically). The microscope may then need to be replaced by some other optical system. As regards its general usefulness, the new method is certainly superior to the classic method, which uses a synchronously revolving mirror and where the object is continuously illuminated. Here, the problem of the synchronous movement of object and mirror has to be solved afresh for every new application. The photographic method compares unfavourably with the present technique because of its slowness — it takes at least a minute to develop a negative — and because of the high costs it entails in photographic material.

There are two other methods based on television techniques, one using a magnetic wheel store on which the picture information is recorded [2]), and the other a storage tube [3]). Compared with our method, however, they both call for much more expensive equipment. Elegant and universally applicable though these systems may be, their use is necessary and justified only in those cases where an inspection time of about 10 seconds is inadequate and where prolonged examination or storage of the pictures is required.

The photographs in *fig. 2* give some idea of the quality of the pictures obtained. Further particulars are mentioned in the caption.

[2]) See J. H. Wessels, A magnetic wheel store for recording television signals, Philips tech. Rev. **22**, 1-10, 1960/61 (No. 1).

[3]) A description of existing types of storage tubes is given by H. G. Lubszynski, in J. sci. Instr. **34**, 81, 1957.

Summary. A set-up is described for examining lamp filaments at the moment they leave the coiling machine, and are thus still in motion. A microscope, focused on the plane in which the coils are moving, produces an enlarged image which is viewed by a vidicon television camera connected to a television receiver. The object is illuminated by a flash-tube. The very short duration of the flash (10 μsec) precludes movement blur. Since the charge pattern on the photoconductive layer of a vidicon decays slowly, it can still be scanned in the normal time (1/25th sec). By using a cathode-ray tube screen of very long afterglow, the picture remains bright enough to be observed for 10 or 15 seconds. The method is potentially applicable to the observation of other moving objects provided an observation time of this order is sufficient.

ABSTRACTS OF RECENT SCIENTIFIC PUBLICATIONS BY THE STAFF OF N.V. PHILIPS' GLOEILAMPENFABRIEKEN

Reprints of these papers not marked with an asterisk * can be obtained free of charge upon application to Philips' Electrical Ltd., Century House, Shaftesbury Avenue, London W.C. 2, where a limited number of reprints are available for distribution.

H 2*: G. Schulten: Novel method for measuring impedances on surface wave transmission lines (Proc. Inst. Radio Engrs. **47**, 76-77, 1959, No. 1).

Brief description of methods of measuring the reflection coefficient of millimetre and sub-millimetre impedances using a microwave reflectometer.

H 3*: H. Severin: Zur Analogie akustischer und elektromagnetischer Randwertprobleme (Acustica **9**, 270-274, 1959, Akust. Beihefte, No. 1). (On the analogy of acoustic and electromagnetic boundary-value problems; in German.)

The conditions for the mathematical analogy of electromagnetic and corresponding acoustic boundary-value problems are investigated. Examples of complete and partial analogy are given. Finally some scalar potential functions are compiled, which are solutions of acoustic boundary-value problems and may be applied to the treatment of corresponding electromagnetic problems.

H 4*: D. Gossel: Die Korrektur des Phasenfehlers von *RC*-Gliedern in der Umgebung ihrer Grenzfrequenz (Arch. elektr. Übertr. **13**, 525-529, 1959, No. 12). (The correction of phase distortion of *RC* networks in the neighbourhood of their cutoff frequency; in German.)

RC networks lose much of their high-pass or low-pass characteristics if they have to be designed for

small phase distortion in the pass band. In this case the distance between transmission-band limit and cutoff frequency becomes very large. A large attenuation results if the networks are used for differentiation or integration and if small phase distortion is required at that. This disadvantage can be greatly reduced if a larger phase distortion is permitted and the latter is then wide-band-compensated by a phase-correcting network. Examples of such phase-correcting networks and the conditions for optimum design are given. For the optimum corrected network and under the condition that flat basic attenuation of 6 dB is tolerated, it is shown that the distance between transmission-band limit and cutoff frequency (high-pass or low-pass filter) or the damping factor (differentiator or integrator), respectively, can be reduced by a factor $2\sqrt[3]{2\psi^2}$, where ψ is the overall phase distortion permitted.

H 5*: F. Karstensen: Über die Diffusion in Germaniumkristallen, die eine Korngrenze enthalten (Z. Naturf. **14a**, 1031-1039, 1959, No. 12). (On diffusion in germanium crystals containing grain boundaries; in German.)

Investigation into the diffusion of donors and acceptors along low-angle tilt boundaries in germanium. The diffusion is examined by measuring the displacement of the *P-N* junction which marks the position of equal donor and acceptor concentrations. The dislocations forming a low-angle tilt boundary act as "diffusion pipes", whereby the diffusion is much faster in the direction of the dislocations than in the normal lattice. Perpendicular to the dislocations this is not so. Diffusion along the dislocations is investigated for As and Sb, for various times and temperatures. It appears that more than one diffusion coefficient is required to describe the diffusion along the grain boundary. From the measurements, and a very rough calculation based on Whipple's formulae, it appears that diffusion along the dislocations is about 10^5-10^6 times faster than in the normal lattice. The diameter of the dislocation pipe is assumed to be six lattice spacings.

H 6*: H. Severin: Sommerfeld- und Harms-Goubau-Wellenleiter im Bereich der Zentimeter- und Millimeterwellen (Arch. elektr. Übertr. **14**, 155-162, 1960, No. 4). (Sommerfeld and Harms-Goubau guides in the cm and mm wave region; in German.)

In addition to well-known numerical results for Sommerfeld and Harms-Goubau guides in the region of decimetre and metre waves the numerical evaluation is extended to centimetre and millimetre waves. Field extent and attenuation as functions of frequency and line data (wire radius, thickness and permittivity of the dielectric coating) are discussed by reference to numerous examples. With tolerable values of field extent, attenuation factors are found that are much smaller than those of hollow metal waveguides of the same frequency range. However, below 5 cm wavelength Sommerfeld and Harms-Goubau guides cannot be used for long-distance transmission if a maximum attenuation of 3.5 dB/km is allowed.

H 7*: G. Schulten: Messung der Eigenschaften von dielektrischen Leitungen bei Millimeterwellen in einem optisch angekoppelten Resonator (Arch. elektr. Übertr. **14**, 163-166, 1960, No. 4). (Measurement of the properties of dielectric rods in the mm-wave region in an optically coupled resonator; in German.)

Dispersion and attenuation of the HE_{11}-mode of the dielectric rod have been measured using the resonator method. The coupling of the resonator has been effected according to optical principles. The coupling element is a nearly transparent mirror consisting of a grid of dielectric threads. Measurements have been made at wavelengths in the 5 and 8 mm region. The dielectric guides were polyethylene threads of various diameters. The deviations of the guide wavelength from the free space wavelength were between 10^{-1} and 10^{-3}%, the attenuation constant in the order of 0.1 dB/m while the radial field extent was about 70 mm.

H 8*: H. Severin: Neuere Entwicklungen der Mikrowellenphysik (Naturwiss. **47**, 217-221, 1960, No. 10). (New developments in microwave physics; in German.)

Discussion of two recent developments in microwave technique. The first concerns the use of ferrites in waveguides for microwave isolators. The phenomena occurring are discussed qualitatively. The author refers to the spin waves that can occur in ferrite materials and to their use for measuring the energy of exchange interactions. The second development concerns parametric amplification which, compared to other methods of microwave amplification, offers the advantage of a lower noise. The principle of parametric amplification is explained and a practical form of such an amplifier using a semiconductor diode is described. Other possibilities of realizing parametric amplifiers are mentioned.

A 19: A. Klopfer: Das Omegatron als Partialdruckmesser (Advances in vacuum science and technology, Proc. 1st int. congress on vacuum techniques, Namur, June 1958, edited by E. Thomas, Vol. 1, pp. 397-400, Pergamon, Oxford 1960). (The omegatron for the measurement of partial pressures; in German.)

A description is given of an omegatron with noble-metal electrodes, which when applying a suitable electrostatic field and with the right kind of cathode enables partial pressures of gases and vapours in the pressure region below 10^{-5} mm Hg to be measured with an accuracy of 10%. The sensitivity of the tube remains constant with time even after prolonged exposure to chemically active gases and vapours such as H_2O, CO_2 and CH_4, and does not depend on the particular tube used as long as the geometrical dimensions are maintained. A comparison of the ionization probabilities taken from the literature with the values calculated from the calibration curves of the omegatron shows that practically all the resonance ions produced by the electron beam are caught by the ion collector. The adjustment of the operating parameters to achieve this is in general independent of the mass.

A 20: E. Baronetzky and A. Klopfer: Einfluss von Gasreaktionen in Vakuumsystemen auf die Zusammensetzung des Restgases (as **A 19**; pp. 401-403). (The influence of gas reactions in vacuum systems on the composition of the residual gas; in German.)

Residual gases in vacuum systems may change their composition either on account of decomposition or because of reaction with components or impurities. The measuring methods often have a marked influence. Care must therefore be exercised when assessing such results. By means of some examples it is shown how the effects of pressure and temperature manifest themselves. Measurements on the kinetics of the decomposition of methane with various cathodes are reported.

A 21: S. Garbe: Restgasanalysen mit dem Omegatron (as **A 19**; pp. 404-409). (Residual-gas analysis with the aid of the omegatron; in German.)

The advantage of the omegatron as compared to other mass spectrometers lies in the possibility of performing gas analyses at very low pressures in a relatively small volume that is cut off from the pump. A description is given of the construction of a glass high-vacuum apparatus, with metal taps, for measurements of gas desorption and for partial-pressure analyses. In the case of permanent gases it was possible to measure gas-desorption rates of a few 10^{-10} torr l/min. The difficulty of determining small amounts of strongly adsorbing gases is explained by the example of water vapour. On account of the chemical reactions at hot surfaces the kind of cathode used in the omegatron and also in ionization manometers has a decisive effect on the result of the analysis. As an example of a residual-gas analysis it is shown how the residual gas above the barium-getter layer of a vacuum tube with an L-cathode alters during operation. (See also Philips tech. Rev. **22**, 195-203, 1960/61, No. 6.)

A 22: A. Klopfer and W. Ermrich: Erfahrungen mit Titan-Ionenpumpen (as **A 19**; pp. 427-429). (Experiences with titanium ion pumps; in German.)

By means of gas analyses with the omegatron, the suitability of the titanium ion pump for use as a high-vacuum pump was investigated. To obtain very low pressures, it became apparent that careful degassing is essential, as for ion and Hg diffusion pumps. Effects that determine the final pressure attainable and the pumping time are reported. (See also Philips tech. Rev. **22**, 260-265, 1960-61 (No. 8.)

A 23: E. Baronetzky: Ein neuartiger, metallischer Getterstoff (Vol. 2 of book mentioned under **A 19**, pp. 646-647). (A new metallic getter material; in German.)

The addition of silver and other noble metals enables the gettering properties of thorium-aluminium alloys at room temperature, in particular the autocatalytic gettering of hydrogen after preliminary oxidation with pure oxygen, and the adsorption of carbon monoxide to be considerably increased. In the Th_2(Al,Ag) system the Th_2Al and Th_2Ag form a continuous series of mixed crystals.

A 24: P. Eckerlin and A. Rabenau: Die Struktur einer neuen Modifikation von Be_3N_2 (Z. anorg. allgem. Chemie **304**, 218-229, 1960, No. 3/4). (The structure of a new modification of Be_3N_2; in German.)

A new hexagonal modification of Be_3N_2 is formed by heating the known cubic form to temperatures above 1400 °C. The transformation is influenced by silicon compounds. The crystal structure of the new modification has been determined by single-crystal X-ray photographs. The space group is P 6_3/mmc. The dimensions of the unit cell containing 2 formula units are $a = 2.841$ Å and $c = 9.693$ Å. There are two kinds of coordination for the Be atoms, viz.

triangular and tetrahedral, the N atoms being then surrounded by five and six atoms, respectively.

A 25: H. G. Grimmeiss, R. Groth and J. Maak: Lumineszenz- und Photoleitungseigenschaften von dotiertem GaN (Z. Naturf. **15a**, 799-806, 1960, No. 9). (Luminescence and photoconductive properties of doped GaN; in German.)

A description is given of a method for the preparation of GaN, which offers the advantage of low working temperature and facilitates doping with a large variety of elements. The luminescence properties of such GaN preparations have been investigated as a function of the preparative conditions, and the emission bands produced by the doping have been determined. In the case of doping with Zn, Cd and Li a level scheme is proposed based on infra-red quenching of fluorescence and the maximum of the emission bands. Glow curves permit of an explanation of the short-wave emissions (so-called satellites) as a trap emission of impurity-containing GaN. In addition a method is described for producing single crystals of GaN, whose photoconductivity was investigated.

Now available:

P. A. Neeteson: Junction transistors in pulse circuits (Philips Technical Library, 1959, pp. viii + 139, 105 figures and 4 plates).

This book forms a companion to the earlier book by the same author, "Vacuum tubes in pulse technique" (Philips Technical Library 1955, second edition 1959). In pulse circuits tubes or transistors are used as switches. Since the transistor is a better approximation than a tube to the ideal switch, transistor pulse circuits are much simpler than the corresponding tube circuits. To keep the treatment brief and simple, the physical background of transistor operation is omitted. The seven chapters of the book are entitled: 1. Introduction; 2. Survey of fundamental pulse circuits; 3. Pulse generators; 4. Pulse shapers; 5. Frequency divider and voltage-level switch; 6. Some auxiliary pulse circuits; 7. Some logic circuits.

The book has also appeared in German.

Harley Carter: An introduction to the cathode ray oscilloscope, second edition (Philips Technical Library, popular series, 1960, pp. 121, 99 figures).

This book explains the operation and design of the cathode ray oscilloscope in non-mathematical language. It is addressed to technicians and shop engineers who are not experts in electronics, and will also appeal to the serious amateur and hobbyist. The chapter headings are as follows: 1. Introduction; 2. The cathode ray tube; 3. The time base; 4. Amplifiers for vertical deflection and pick-ups for converting non-electrical phenomena into electrical magnitudes; 5. Power supply for cathode ray oscilloscopes; 6. Practical applications of the oscilloscope; 7. Standard cathode ray tubes for oscillography; 8. Some complete oscilloscope circuits.

E. Rodenhuis: Hi-Fi amplifier circuits (Philips Technical Library, popular series, 1960, pp. x + 105, 64 figures).

Until a few years ago the high-fidelity reproduction of sound was an ideal attainable only by enthusiasts with expensive equipment. The situation is now considerably improved in that the price of quality has dropped very considerably, which has brought Hi-Fi within the reach of a much wider circle.

The book noticed here is a companion to "Electron tubes for A.F. amplifiers" by the same author (Philips Technical Library, popular series, 1960). It deals in detail with a number of amplifier circuits of very high quality which can be built at a reasonable cost. The three chapters of the book are: 1. General considerations on the design of Hi-Fi amplifiers; 2. Power amplifier circuits; 3. Pre-amplifiers.

P. van der Ploeg: Industrial electronics apparatus — steps in design and maintenance (Philips Technical Library, popular series, 1960, pp. xi + 97, 20 figures, 33 plates).

The object of this book is to show how the trouble-free operation of electronic equipment is dependent on details of its design, manufacture, use and maintenance. The book includes many practical tips and hints of value to both designers and service engineers. The chapters are: 1. The function of the equipment; 2. The laboratory test; 3. The prototype; 4. Production; 5. Installing the equipment; 6. The purpose of maintenance; 7. Maintenance; 8. Fault finding. A supplement, "Electronic tube data", at the end of the book forms a brief guide to the use of tube characteristics, operating data and limiting values.